Design and development of solid-state nanostructures for catalysis

Franzén, Sara

2023

Document Version:
Publisher's PDF, also known as Version of record

Design and development of solid-state nanostructures for catalysis

SARA M. FRANZÉN
DEPARTMENT OF PHYSICS | FACULTY OF ENGINEERING | LUND UNIVERSITY

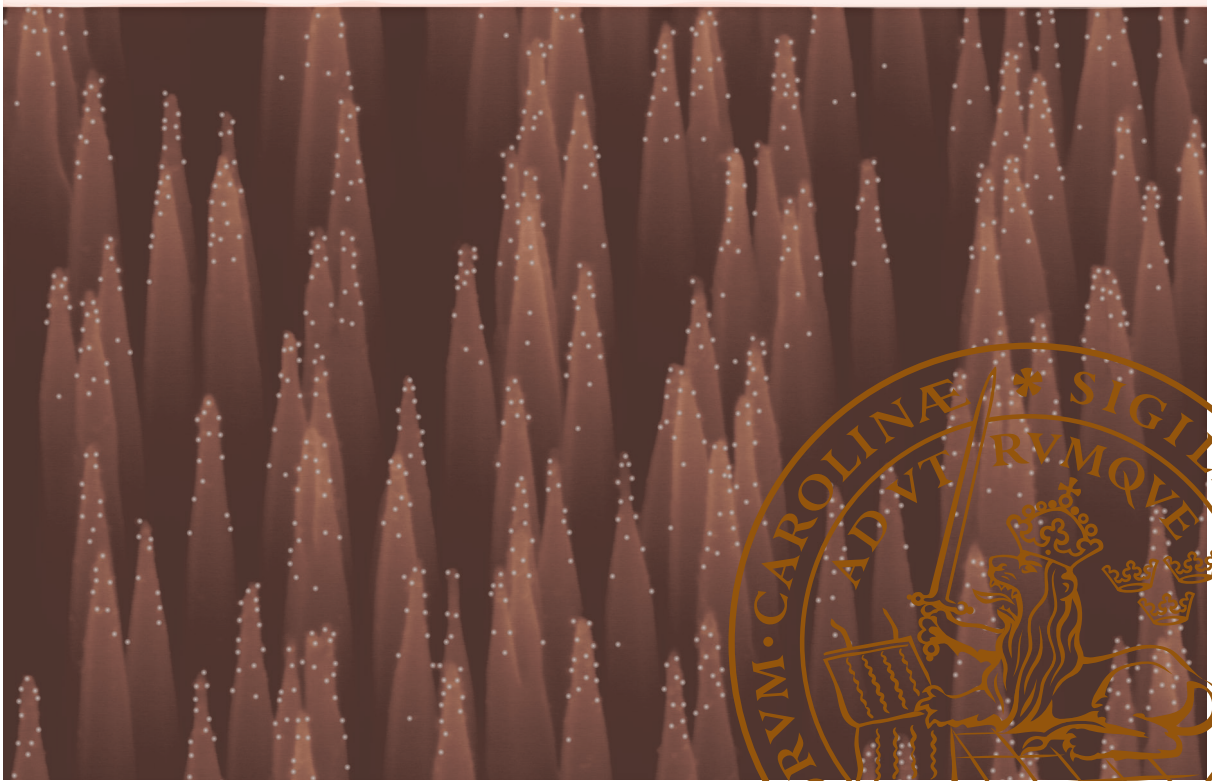

Design and development of solid-state nanostructures for catalysis

Design and development of solid-state nanostructures for catalysis

by Sara M. Franzén

LUND
UNIVERSITY

DOCTORAL DISSERTATION
Thesis advisors: Maria E. Messing, Martin H. Magnusson, and Daniel Strand
Faculty opponent: Andreas T. Güntner

To be presented, with the permission of the Faculty of Engineering of Lund University, for public criticism in the Rydberg hall at the Department of Physics on Friday, the 15th of December 2023 at 09:15.

Organization
LUND UNIVERSITY

Department of Physics
Box 118
SE–221 00 LUND
Sweden

Document name
DOCTORAL DISSERTATION

Date of disputation
2023-12-15

Sponsoring organization

Author(s)
Sara M. Franzén

Title and subtitle
Design and development of solid-state nanostructures for catalysis

Abstract
Catalytic processes are present in a wide range of aspects, from fundamental biological processes to modern chemical synthesis. In practical terms, catalysis has thrived as a rapidly growing industry. However, a significant gap in our understanding of catalytic processes exists between the molecular and industrial scales, arising from the complexity at the nano- and micro-levels of catalytic nanoparticles and their supports. Heterogeneous catalysts, where the catalyst is in a different phase than the reactants, are widely used due to their ease of retrieval from reaction mixtures. However, they typically require high temperatures and pressures to operate efficiently. Enhancing the efficiency of heterogeneous catalysts under milder conditions could have significant environmental and economic benefits.

In this thesis, a novel approach to designing and developing solid-state nanostructures for catalysis is presented. It encompasses three main components: the generation of catalytic nanoparticles, the fabrication of nanostructure supports, and post-processing techniques to enhance stability. Aerosol methods, specifically spark discharge generation, are employed to produce nanoparticles with high control over size, composition, and crystallinity. The fabrication of support structures, using epitaxial growth, resulted in close-packed tapered gallium phosphide nanowires and nano-trees that elevate catalytic nanoparticles, enhancing their accessibility to reactants during reactions. The thesis also addresses the challenge of stability for the catalytic nanoparticles in reaction environments, both for the use of planar supports and with high-aspect-ratio nanowire supports. The work includes the development of a method to study stability under reaction conditions, enabling the determination of suitable material systems. Finally, the catalytic evaluation of nanowire-supported palladium nanoparticles reveals promising results for the nanostructured catalysts, with a 15-fold increase in catalytic activity compared to using a planar support.

Key words
catalysis, nanoparticles, spark ablation, bimetallic, nanowires, epitaxy, hydrogenation

Classification system and/or index terms (if any)

Supplementary bibliographical information

Language
English

ISSN and key title

ISBN
978-91-8039-890-9 (print)
978-91-8039-891-6 (electronic)

Recipient's notes

Number of pages
179

Price

Security classification

Signature

Date 2023-11-06

Design and development of solid-state nanostructures for catalysis

by Sara M. Franzén

LUND
UNIVERSITY

Cover photo by Sara M. Franzén and Ellinor Huss

Faculty of Engineering, Department of Physics

ISBN: 978-91-8039-890-9 (print)
ISBN: 978-91-8039-891-6 (electronic)

Printed in Sweden by Media-Tryck, Lund University, Lund 2023

Dedicated to my family
Mathias – Love – Ilse

Contents

Abstract

Catalytic processes are present in a wide range of aspects, from fundamental biological processes to modern chemical synthesis. In practical terms, catalysis has thrived as a rapidly growing industry. However, a significant gap in our understanding of catalytic processes exists between the molecular and industrial scales, arising from the complexity at the nano- and micro-levels of catalytic nanoparticles and their supports. Heterogeneous catalysts, where the catalyst is in a different phase than the reactants, are widely used due to their ease of retrieval from reaction mixtures. However, they typically require high temperatures and pressures to operate efficiently. Enhancing the efficiency of heterogeneous catalysts could have significant environmental and economic benefits.

In this thesis, a novel approach to designing and developing solid-state nanostructures for catalysis is presented. It encompasses three main components: the generation of catalytic nanoparticles, the fabrication of nanostructure supports, and post-processing techniques to enhance stability. Aerosol methods, specifically spark discharge generation, are employed to produce nanoparticles with high control over size, composition, and crystallinity. The fabrication of support structures, using epitaxial growth, resulted in close-packed tapered gallium phosphide nanowires and nano-trees that elevate catalytic nanoparticles, enhancing their accessibility to reactants during reactions. The thesis also addresses the challenge of stability for the catalytic nanoparticles in reaction environments, both for the use of planar supports and with high-aspect-ratio nanowire supports. The work includes the development of a method to study stability under reaction conditions, enabling the determination of suitable material systems. Finally, the catalytic evaluation of nanowire-supported palladium nanoparticles reveals promising results for the nanostructured catalysts, with a 15-fold increase in catalytic activity compared to using a planar support.

Popular summary in English

Catalysis permeates most aspects of our world here on Earth. In our bodies, catalysts are called enzymes and play a crucial role in allowing us to extract energy from the food we eat, among other, more or less vital, functions. In industry, catalysts are used both in the production of automotives' fuel and in cleaning emissions from their combustion, in the manufacture of medicines and vitamins, as well as in a wide range of other processes for producing everything from plastics to fertilizers. Catalysis is a well-explored subject thanks to its practical applications, but due to its complexity, there is still much we do not understand. If we can increase our understanding, there is the potential to save a lot of energy and money in a wide range of manufacturing processes.

So – what is a catalyst? A catalyst is a substance that changes the speed of a reaction without being consumed itself. Often, one wants to speed up a reaction to produce more material in a certain time or to run the reaction at a lower temperature and/or pressure, thus saving energy in the production. The catalyst accomplishes this by allowing the molecules that are to react to attach to its surface, and when they do, the bonds between the atoms in the molecules weaken, making it easier for them to react with each other and form a new molecule, as illustrated in Figure 1.

The catalyst can be a molecule, an enzyme, or, as in this thesis, a metal. Good catalysts are often noble metals like platinum and palladium. However, these metals are expensive, so there is an interest in reducing the amount of material required. Since reactions occur on the surface of the catalyst, all material that is not surface is unnecessary. Therefore, nanoparticles are often used for catalysis

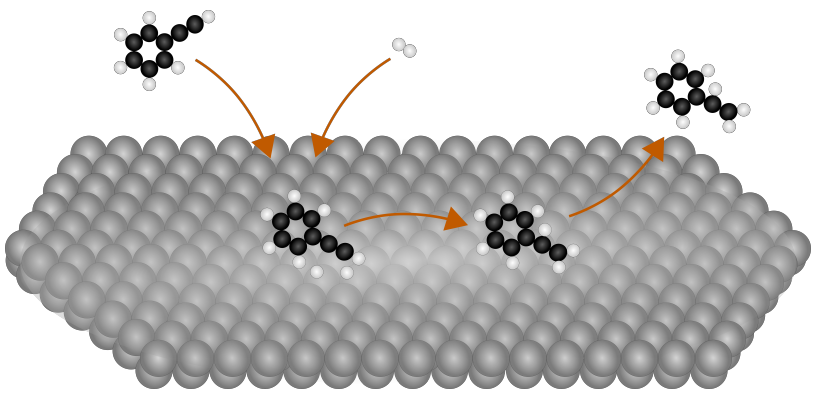

Figure 1: Illustration of the catalytic process where two molecules adsorb onto the surface and react with each other to form a new molecule that subsequently desorb from the surface.

because they have more surface area per gram (or microgram) of metal compared to larger particles. For example, a 10 mm particle has a surface-to-volume ratio of 600 m^2/m^3, while a 10 nm particle has a surface-to-volume ratio of 600,000,000 m^2/m^3. It is clear that using nanoparticles is an effective way to get a lot of surface area from one's material.

As already mentioned, the choice of metal is important for how the catalyst functions for different reactions, and the possibilities are nearly endless. In this work, we have used aerosol methods to generate nanoparticles, specifically one called the spark discharge generator, where nanoparticles are created when sparks strike between two metal rods. The particles consist of the same material as the rods, and it is possible to mix and match materials as you like to create bimetallic nanoparticles, particles consisting of two different metals. These particles have entirely new properties compared to pure metals, and these properties have been investigated in this thesis.

One problem with nanoparticles is that they tend to stick to any surface they come into contact with, including other nanoparticles. Therefore, it is practical to have the particles attached to a well-chosen surface so that they can be easily handled and moved, for example, to and from the container where the chemical reaction is to take place. A commonly used support is powder of some material that is not itself catalytically active, such as silicon oxide. The problem with powders is that they are random in their structure, which means that some nanoparticles will be well-positioned to participate in the reaction, while others will be hidden and therefore not contribute to the same extent. This makes it difficult to determine exactly how good catalysts the nanoparticles are. In this work, I have looked for more precise information about the catalyst's performance to better understand how it works and, ultimately, to influence how it works. For this purpose, I have developed so-called nanostructures as supports for the catalytic nanoparticles. The technique used to grow these nanostructures offers flexibility to adjust the structures with high precision.

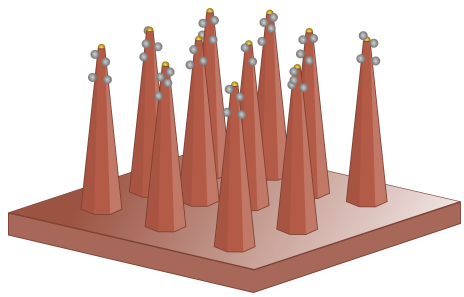

Figure 2: Catalytic nanoparticles attached on well-defined nanostructures.

The result was a forest of nanotrees adorned with catalytic nanoparticles, and how well they perform - you can read about in the thesis!

Populärvetenskaplig sammanfattning på svenska

Katalys genomsyrar det mesta i vår värld här på jorden. I vår kropp kallas katalysatorerna för enzymer och spelar en avgörande roll för att vi ska kunna tillgodogöra oss energi från maten vi äter samt andra mer eller mindre livsviktiga funktioner. Inom industrin används katalysatorer både vid tillverkning av bilar bränsle och för att rena avgaserna vid dess förbränning, vid framställning av mediciner och vitaminer samt vid en stor mängd andra processer för framställning av alltifrån plaster till gödningsmedel. Katalys är ett väl undersökt fenomen tack vare dess praktiska tillämpningar men på grund av dess komplexitet så är det mycker vi fortfarande inte förstår. Om vi kan öka vår förståelse så finns det möjlighet att spara mycket energi och pengar i en lång rad av tillverkningsprocesser.

Så vad är egentligen en katalysator? En katalysator är någonting som ändrar farten på en reaktion utan att själv förbrukas. Ofta vill man snabba upp en reaktion för att kunna producera mer material på en viss tid, eller för att kunna köra reaktionen vid en lägre temperatur och/eller tryck och därmed spara energi vid produktionen. Det här åstadkommer katalysatorn genom att låta molekylerna som ska reagera att fästa vid dess yta och när de gör det så försvagas bindingarna mellan atomerna i molekylerna vilket gör att de lättare kan reagera med varandra och bildar en ny molekyl, som illustrerat i Figur 1.

Katalysatorn kan vara en molekyl, ett enzym eller, som i den här avhandligen, en metall. Bra katalysatorer är ofta ädla metaller som platina och palladium. Dessa metaller är dock dyra och det finns därför ett intresse av att minska mängden material som behövs. Eftersom reaktionerna sker på ytan av katalysatorn är allt

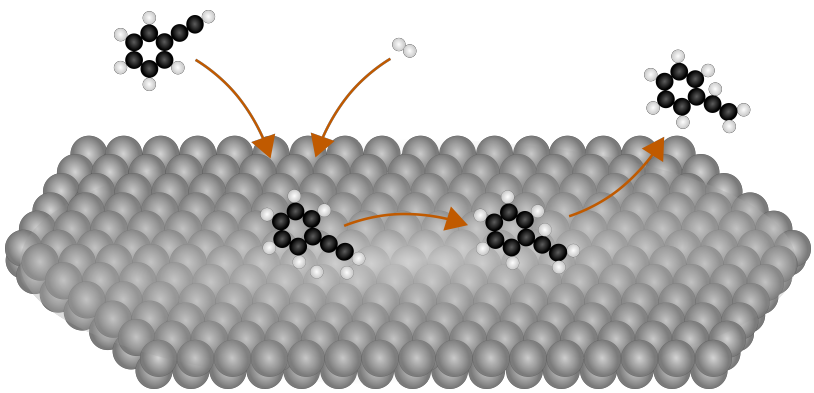

Figur 1: Illustration av den katalytiska processen där två molekyler fäster vid ytan, reagerar med varandra för att bilda en ny molekyl som sedan släpper från ytan.

material som inte är yta onödig. Därför används ofta nanopartiklar för katalys, eftersom de har mer yta per gram (eller mikrogram) metall, jämfört med större partiklar. Till exempel, en partikel som är 10 mm har en yta-till-volym-ratio på 600 m^2/m^3 medan en partikel som är 10 nm har en yta-till-volym-ratio på 600.000.000 m^2/m^3. Det är tydligt att användning av nanopartiklar är ett effektivt sätt att få mycket yta från sitt material.

Som redan nämnt är valet av metall viktigt för hur katalysatorn fungerar för olika reaktioner, och här är möjligheterna näst intill oändliga. I det här arbetet har vi använt oss av aerosolmetoder för att generera nanopartiklar, specifikt en som kallas gnistgeneratorn där nanopartiklar skapas när gnistor slår mellan två metallstavar. Partiklarna består av samma material som stavarna och här kan man mixa och matcha material lite som man vill för att skapa bimetalliska nanopartiklar, dvs partiklar som består av två olika metaller. Dessa partiklar får helt nya egenskaper jämfört med de rena metallerna och de här egenskaperna har undersökts i den här avhandlingen.

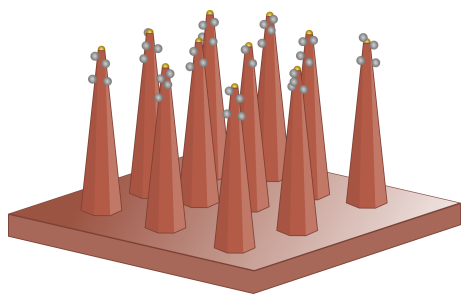

Figur 2: Katalytiska nanopartiklar fästa på väldefinierade nanostrukturer.

Ett problem med nanopartiklar är att de tenderar att fastna på vilken yta de än kommer i kontakt med och även i varandra. Därför är det prakiskt att ha partiklarna fästa på en väl vald yta så att man enkelt kan hantera och förflytta dem, t ex till och från behållaren där den kemiska reaktionen ska ske. Ett underlag som ofta används är pulver av något material som inte själv är katalytiskt aktiv, t ex kiseloxid. Problemet med pulver är att de är slumpartade i sin struktur vilket innebär att vissa nanopartiklar kommer hamna väl tillgängliga för att delta i reaktionen, medans andra kommer att hamna undangömda och därmed inte bidra i samma utsträckning. Detta gör det svårt att avgöra exakt hur bra katalysatorer nanopartiklarna är. I det här arbetet har jag varit ute efter mer precis information om katalysatorns prestanda för att bättre förstå hur den fungerar och, i förlängningen, kunna påverka hur den fungerar. För det här syftet har jag utvecklat så kallade nanostrukturer som underlag till de katakytiska nanopartiklar. Tekniken som används för att växa de här nanostrukturerna erbjuder en flexibilitet för att kunna justera strukturerna med hög precision.

Resultatet var en skog av nanoträd dekorerade med katalytiska nanopartiklar, och hur väl de fungerar – det kan ni läsa om i avhandligen!

Acknowledgements

I am grateful for the opportunity to formulate my acknowledgements toward the people who have been important for me during my doctoral studies. The road towards a PhD is a special one, exploratory and sometimes veiled, and it is nice to walk it alongside good people.

Maria Messing – you have taught me so much, about research, ethics, and communicating science, and about the importance of allowing room for personal interests and family. Martin Magnusson – thank you for trusting me with this project and for all the fun conversations about research, language, and life in general. Daniel Strand – you have inspired me with your clear vision, which has been very important for me when the path forward was difficult to see.

When I first started, it was not clear (at least not to me) that I would be a part of the aerosol group. My project was cross-disciplinary and without an apparent belonging, but I am very glad to have had my base in this group. Markus, Marie, Pau, Linnéa, Mehran, Knut, Thomas, Sudha, Calle, Namsoon, Robert, Linus. I can not imagine a better research group. Thank you for all the great discussions and team work in the lab. Special thanks to Bengt for all the help with the aerosol tools, I don't know what I would have done without you.

My other belonging has been with the Strand group at CAS, where I have been impressed by the skilled organic chemists that I have had the pleasure of working with. Christian, you were there during the first attempts of catalysis with my strange nanostructures. Magdalena, you took our catalysis work to the next level and I really enjoyed working on this project with you. Leonard, you joined last year and it has been nice getting to know you and working with you. I appreciate your curious mindset and cool research ideas.

I have been in the same office throughout my time at FTF, until about a week ago when we had to move. During this time there have been a few people residing in the office with me with whom I have had the pleasure of discussing everything and anything with: Subhomoy, Mikkel, Enrico, Mohammed, and Sudha – you get mentioned twice, which is well deserved. Thank you for being such a good friend.

Before I started my PhD, I always thought that FTF was the coolest division and I still believe this to be true. Sure, because of the science, but specially because of the people! Dan Hessman, you are the key person that shapes this division with enthusiasm and dedication, for which I am very grateful. Fellow PhD students and post-docs who have made this place great: Oskar, Jonathan, Lukas, Irene,

Anette, Florinda, Neimantas, Damiano, David, Thanos, Markus, Matteo, Max, Patrik, Ruby, Therese, William, Kristi, Harald, Yue, Antti, Asmita, Hossein, Vanya, Julia, Mariapia, Pradheebha, Simon, Stephanie.

Finally, I would like to thank my family. My parents and brothers, thank you for listening to it all, good and bad. Love and Ilse, thank you for being the most important thing in my life, putting everything else in perspective. Mathias, thank you for your endless support. Without you, this would not have been possible.

List of publications

This thesis is based on the following publications, referred to by their Roman numerals:

I **Compositional tuning of gas-phase synthesized Pd-Cu nanoparticles**
S.M. Franzén, L. Jönsson, P. Ternero, M. Kåredal, A.C. Eriksson, S. Blomberg, M.E. Messing
Nanoscale Advances (2023)

I conceived the study together with co-authors, performed the experiments, and analyzed the data together with co-authors. I wrote the paper with contributions from all authors.

II **Branched-gallium phosphide nanowires seeded by palladium nanoparticles**
M. Bermeo, **S.M. Franzén**, C. Hetherington, J. Johansson, M.E. Messing
Nanotechnology, 34, 395603 (2023)

I developed the growth recipe for the gold-seeded growth, took part in discussions regarding the Pd-seeded growth, and took part in the discussions regarding the results and analysis. MB conducted the Pd-seeded growth and performed the TEM. I contributed to the writing of the paper.

III **Stability of supported aerosol-generated nanoparticles in liquid media**
S.M. Franzén, M. Tasić, C.B.M. Poulie, M.H. Magnusson, D. Strand, M.E. Messing
Scientific Reports, 11, 9276 (2021)

I conceived the study together with co-authors, performed the experiments and analyzed the data together with co-authors. I wrote the paper with contributions from all authors.

IV **Nanowire-supported palladium nanoparticles for hydrogenation reactions**
S.M. Franzén*, L. Schilling*, M. Bermeo, M. Tasić, M.H. Magnusson, M.E. Messing, D. Strand
In preparation

* These authors contributed equally.

I conceived the study together with co-authors and developed and characterized the catalysts. LS and MT performed the catalytic evaluation. I contributed to discussions and writing as shared first author.

All papers are reproduced with permission of their respective publishers.

Publications not included in this thesis:

V **Emissions and exposures of graphene nanomaterials, titanium dioxide nanofibers, and nanoparticles during down-stream industrial handling**
K. Lovén, **S.M. Franzén**, C. Isaksson, M.E. Messing, J. Martinsson, A. Gudmundsson, J. Pagels, M. Hedmer
Journal of Exposure Science & Environmental Epidemiology (2021)

VI **Bimetallic Nanoparticles as a Model System for an Industrial NiMo Catalyst**
S. Blomberg, N. Johansson, E. Kokkonen, J. Rissler, L. Kollberg, C. Preger, **S.M. Franzén**, M.E. Messing, C. Hulteberg
Materials (2019)

Chapter 1

Introduction

Catalytic processes pervade most aspects of life on this Earth, from fundamental biological processes to modern chemical synthesis. Catalysis is conceptually well-understood on the molecular level due to the advancement of surface science techniques and computational chemistry [1, 2]. Furthermore, it is practically highly developed as catalysis has been a large and rapidly growing industry ever since the development of the ammonia synthesis in the early 20^{th} century [3]. However, between these two regimes, the field possesses a huge gap in understanding because of the complexity that arises on the nano- and micro-level of catalytic nanoparticles and their supports [4].

Understanding the relationship between the structure of a catalyst and its performance during a reaction is paramount in comprehending catalysis as a whole. To unravel the intricate mechanisms underlying catalytic reactions, researchers have employed a wide array of techniques to study the processes occurring on the surface of the catalyst [5]. However, the study of catalytic processes on the surface of a catalyst poses significant experimental challenges. Catalytic characterization necessitates the investigation of catalyst behavior under various reaction conditions, including different pressures and temperatures. These conditions are crucial factors that influence the catalyst's activity, selectivity, and stability. Bridging the gap between fundamental studies conducted on single crystals in ultrahigh vacuum environments and the practical demands of high-pressure industrial processes represents a significant challenge in the field of nanocatalysis [6].

In principle, there are two directions in catalysis research — heterogeneous and homogeneous — the heterogeneous catalyst is in a different phase as the re-

actants, typically a solid catalyst and liquid or gas-phase reactants; and the homogeneous catalyst is in the same phase as the reactants, such as molecular complexes in solution [7]. Heterogeneous catalysts are practical to work with as they are easily retrievable from the reaction mixture and does thus not generate issues with separation between metallic species and product, something that is a key issue with homogeneous catalysts. However, a drawback of heterogeneous catalysts is that they typically require high temperatures and pressures to operate efficiently and it was not until the development of nanoscience in the 1990s that supported nanoparticle catalysts was developed to withstand the high pressures associated with industrial production [8]. Due to these high temperatures and pressures, there is a lot to gain, both environmentally and financially, by increasing the efficiency of heterogeneous catalysts.

1.1 Nanostructures for catalysis

Heterogeneous catalysis takes place on surfaces. Thus, in order to increase the frequency of catalytic events, nanostructures can be used to maximize the amount of exposed surface. As an example, consider a piece of catalytic material with the dimensions 1x1x1 mm which has a surface area is 6 mm^2 and a volume of 1 mm^3. However, using the same volume to make nanoparticles with a radius of 10 nm would result in a total surface area of about 600,000 mm^2. Clearly this is a more efficient use of the expensive catalytic material.

Nanocatalysts offer more than just an increase in surface area. The ability to manipulate the size of the catalytic structures grants the power to modify the catalytic properties of the surface. Scaling down in size allows for the manipulation of structural properties, including shape, morphology, and phase of the catalyst [9–11]. Such properties affect various aspects of the catalyst's surface, such as the coordination environment, valence state, and geometric configuration of the active sites which will have a substantial impact on the reaction rate and selectivity for a specific chemical transformation. Additional tailoring of the catalytic performance can be achieved by the use of bimetallic materials which enable variation of chemical composition [12, 13]. The ability to control these key parameters at the nanoscale offers immense potential for designing highly efficient and selective catalysts for a wide range of chemical processes.

In heterogeneous catalysis research, the catalysts are commonly composed of metal nanoparticles supported on a high-surface-area material, such as carbon, zeolites, or metal oxides [14]. The high-surface-area material is typically prepared using various methods like precipitation, sol-gel, impregnation,

or deposition, while the active components are introduced onto the support material through impregnation, deposition-precipitation, or other techniques. Such conventional methods exhibit certain drawbacks. Firstly, these methods lack control over the precise positioning of particles on the support, leading to random distribution and varying accessibility of nanoparticles to reactants. Consequently, the resulting catalytic response represents an average of multiple positions. Secondly, these methods involve the use of different chemicals and components, increasing the likelihood of introducing contaminants into the final catalyst product. These limitations highlight the need for advanced synthesis techniques that offer better control over particle distribution and minimize the introduction of unwanted impurities, ultimately leading to a better understanding of the mechanisms behind catalytic activity and selectivity.

1.2 Solid-state synthesis methods for fabrication of nano-catalysts

Using physical methods and nanofabrication methods to synthesize solid-state catalyst allows for high structural precision with small variations over large surfaces. This enables detection of small variations in the catalytic morphology. Furthermore, contamination can be kept at a very low levels if the fabrication takes place in a gaseous environment as it is easier to keep at high purity compared to a liquid environment.

Physical methods for nanoparticle production can achieve a higher purity than chemical methods since no liquid chemicals are involved. The physical methods used for the work presented in this thesis are often referred to as aerosol methods as the processes involves condensation of a vapor in an inert gas, resulting in nanoparticles suspended in a gas — an aerosol. The vapor can be generated in various ways, e.g., by laser ablation [15], arc discharges [16], or, as in this

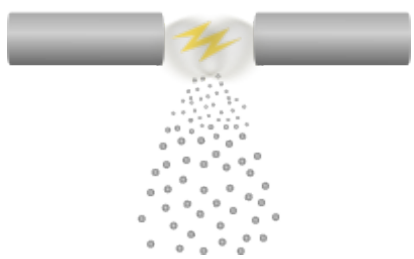

Figure 1.1: Nanoparticle generation by spark discharges. Small primary particles are formed directly after the spark which coalesce and grow into larger nanoparticles.

thesis, thermal evaporation [17] or spark discharges [18]. The primary particles that are formed immediately after the spark due to the rapid temperature gradient will coalesce and grow into larger nanoparticles (Figure 1.1) and the final size distribution can be controlled by changing parameters such as carrier gas flow, spark energy and frequency (for vapor generated by spark discharges), and temperature (for vapor generated by thermal evaporation) [17, 19, 20]. Further manipulation of size distribution, oxidation state, and crystallinity can also be done using common aerosol instruments [21].

Particle-assisted epitaxial growth of compound semiconductor nanostructures has been an important processing method for the support development. Epitaxial growth of nanostructures is well understood because of the intense research on the subject in the past decades [22–24]. A myriad of applications have sprung that are based on one-dimensional nanostructures called nanowires, such as solar cells, micro-LEDs, and sensors for diagnostics [25–27]. In this thesis, the fairly unexplored application of nanowires as supports for catalytic nanoparticles is studied. The purpose is to take advantage of the mature field of nano-processing that can provide highly controlled structures on the nanoscale. These can be used to study nanoparticle-support interaction and other possible synergy effects.

1.3 Scope of the thesis

The work in this thesis aims to design and develop solid-state nanostructured catalysts that can be used to gain understanding of heterogeneous catalysts. The catalysts I developed in this work are model catalysts fabricated with a modular approach, so that the catalytic nanoparticles and their support can be modified independently. The catalytic nanoparticles were generated using an aerosol method, which provided a high versatility in regards to size distribution, crystallinity, and chemical composition. This, in combination with the nanoprocessing techniques used to develop the supports, has facilitated the fabrication of highly specialized catalysts. For all of these development steps it has been vital to use a number of different characterization methods, which will be described in **Chapter 2**.

The rest of this thesis is organized by the different components of the nanocatalysts, starting with the generation of aerosol nanoparticles in **Chapter 3**. In this chapter I also present my work on compositional tuning of Pd-Cu bimetallic nanoparticles (**Paper I**), which are interesting for catalytic application because of the synergistic effects of palladium and copper.

The supports were fabricated using epitaxial growth, specifically metal-organic vapor phase epitaxy of tapered gallium phosphide nanowires. These support structures would serve by elevating the catalytic nanoparticles, increasing their accessibility to the reactants during reaction. The design and development of these structures, starting from gold-seeded nanowires and ending up with palladium-seeded nanotrees (**Paper II**), are presented in **Chapter 4**.

Because of the novel nature of the approach used here, there were many unknowns in the beginning of the project. For example, the use of semiconductor nanostructures in combination with aerosol-generated nanoparticles was new and their stability in reaction conditions were not known. This stability is extremely important for the application of catalysis, and is treated in **Chapter 5**. In the first part of the chapter, based on **Paper III**, a method was developed to study the stability of supported aerosol-generated nanoparticles, based on a combination of identical-location scanning electron microscopy and size and density analysis to detect any changes in the samples before and after exposure to common reaction conditions. This method could then be used to determine suitable reaction conditions for the material systems I developed. In the second part of the chapter I discuss the challenge when using high-aspect ratio nanostructures in the relatively harsh conditions in which catalytic reactions take place, specifically, the mechanical and chemical stability of the structures.

In **Chapter 6** I finally review the catalytic performance of the developed nanostructures. This chapter is based on **Paper IV** and includes the optimization study, kinetics evaluation, and three phase test of heterogenicity. Following this is the final **Chapter 7**, which includes my conclusions on the work presented in this thesis, along with an outlook for the future work on this subject.

Chapter 2

Materials characterization

Working with material science, and specifically with nanostructures, some information can be acquired by looking at a sample with the naked eye. For example, when growing gallium phosphide (GaP) nanowires on a planar GaP substrate, the polished, light orange, semi-transparent surface is replaced by a matte, darker, opaque surface and the shade of orange will depend on the length and thickness of the nanowires. Thus, a first estimate of whether a change in the growth recipe has had any effect can be achieved immediately. However, in order to gain deeper, more detailed information regarding the sample, such as morphology, chemical composition, and crystal structure, a wide range of tools and techniques can be applied. In this chapter, a selection of microscopy and spectroscopy techniques will be described.

2.1 Electron microscopy

Conventional optical microscopes, which the term microscopy most often refers to, do often not have sufficient resolving power for imaging nanostructures. In an optical microscope, visible light and optical lenses are used to magnify an object so that small features can be observed and imaged. However, due to diffraction effects, the resolution of microscopes is limited to about half of the wavelength of the light used, although there are different techniques used in optical microscopy to overcome this limitation to some degree [28, 29]. In order to achieve the resolving power necessary to successfully study nanostructures, electrons are used. Electrons have wavelength of a few picometer (1 pm = 10^{-3} nm) when accelerated to the energies typically used in an electron microscope. The

wavelength is thus no longer the limiting factor. There are two main types of electron microscopes (with a myriad of variations): The scanning electron microscope (SEM), which is an excellent tool for shape and size characterization of nanostructures, with nanometer resolution [30]; and the transmission electron microscope (TEM), in which features down to the atomic level can be resolved, making the tool ideal for studying the crystal features of nanostructures or particles [31].

Early development of electron microscopy took place in the beginning of the 20th century and for this work, Ernst Ruska received the Nobel Prize in Physics in 1986 [32]. Since then, the energy of the electron beam has been increased from 300 eV to about 300 000 eV in a typical transmission electron microscope and more advanced features have been added in order to achieve higher resolution, although the principle is still the same. The electron microscope consists of an electron gun, where electrons are generated, and accelerated by an electric field. The electron beam is focused by electromagnetic lenses and directed towards the sample.

In a *scanning electron microscope* (SEM) electrons are accelerated to an energy of 0.1–30 keV and focused using electromagnetic lenses to a single spot on the sample, resulting in emission of secondary electrons and backscattered electrons

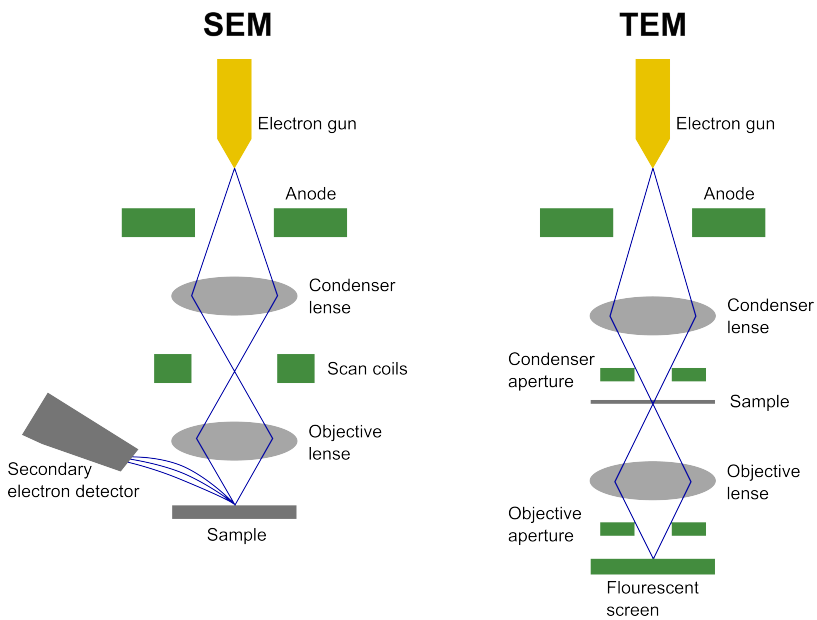

Figure 2.1: Schematics of an SEM and a TEM, highlighting the similarities and the differences of the two microscope types.

from the excited region [33]. As the focused electron beam is scanned over the imaged area by scan coils, the emitted electrons are collected by a detector and an image is created from the intensity of emitted electrons from each position of this area. Depending on the detector used, different information can be deduced, from more topological to more compositional [34]. A simplified schematic of the SEM can be found in figure 2.1 which illustrates the key elements of the tool.

For a *transmission electron microscope* (TEM) the resolving power is increased significantly compared to the SEM as the electrons are accelerated to reach an energy of about 100–400 keV [35]. The resolution is also enhanced by the fact that the electrons are transmitted through the specimen (that must be thin, below about 100 nm, or below 50 nm for high-resolution imaging), which means that the high electron energy will not contribute to a large excitation volume, as would be the case in an SEM. The sample is placed above the objective lens and the electrons are irradiated through the sample and an image is projected on a fluorescent screen. This means that the sample needs to be prepared, either by using a thin self-supporting specimen or by depositing the specimen onto a supporting grid designated for the TEM. A supporting grid typically consists of a metal grid onto which there can be a thin film, e.g. amorphous carbon. The grid often consist of copper, but other metals can also be used. The specimen preparation, the high energy electron beam, and the advanced correctors all contribute to enhancing the resolution of the TEM, enabling atomic resolution.

A TEM can also be equipped with the hardware and software required for scanning TEM (STEM). In this mode the beam is made even finer and advanced objectives are used to scan the sample, while keeping the incidence of the beam parallel to the optical axis. In this work, the STEM mode has mostly been used as a ground for analytical electron microscopy. There are several analytical techniques related to transmission electron microscopy, but the one that is most relevant to and extensively used in this thesis is *energy-dispersive X-ray spectroscopy* (EDXS), which will be discussed in the section below.

2.2 Spectroscopy and diffraction

Spectroscopy methods enable the collection of chemical information about a sample by irradiation of electromagnetic radiation or electrons while recording the energy of the absorbed or emitted radiation [36]. It is the study of the interaction between the radiation and the matter and, depending on the type of spectroscopy, information regarding chemical composition, and physical and electronic structure can be provided.

For the results presented in this thesis, a few different spectroscopy methods have been used. EDXS, as mentioned in the previous section is often used in a (S)TEM. As the sample is irradiated with electrons in the TEM or STEM mode (TEM-EDXS or STEM-EDXS), secondary electrons are generated and leave vacancies. These vacancies are consecutively refilled by electrons from higher energy levels and X-rays with an energy equal to the difference between the two energy levels are emitted (Figure 2.2a). These X-rays can be detected to generate a spectrum from which chemical information about the sample can be deducted.

X-ray fluorescence (XRF), a high precision analysis method for determining the elements present in a sample [37], was used for the evaluation of bimetallic nanoparticles. XRF has a similar working principle as (S)TEM-EDXS, although with the difference that the vacancies are created when irradiating the sample with X-rays instead of with electrons (Figure 2.2b). When the sample is irradiated the atoms in the sample are set into an excited state. As the atoms relax into their ground state, radiation is emitted and measured by a spectrometer.

In *X-ray photoelectric spectroscopy* (XPS) the photoelectric effect is employed to study the binding energy of the core level electrons of a material [38]. As the sample is irradiated by X-rays, photoelectrons are emitted (Figure 2.2c). The

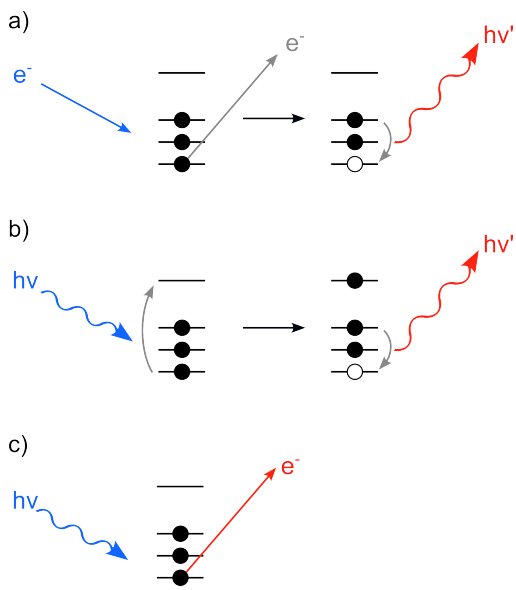

Figure 2.2: Visualization of the working principles of the spectroscopy methods a) (S)TEM-EDXS, b) XRF, and c) XPS, showing the incoming radiation in blue and the measured radiation in red, and the effect on occupancy of the energy levels as a result of the interaction between the radiation and the matter.

emitted electrons will have a kinetic energy energy, KE, equal to the difference between the photon energy, νh, and the energy required for ionization, i.e. the binding energy, BE, plus the working function ϕ:

$$KE = \nu h - (BE + \phi) \tag{2.1}$$

The resulting core level spectra provide information about the atoms in the material and their chemical environment. The method is highly surface sensitive due to the short mean free path of the electrons in solid materials, making it suitable to study catalysts, for which the surface is the significant feature.

By studying diffraction, information regarding chemical composition and crystal phase of a sample can be gained. A diffraction pattern is generated as radiation (typically X-rays or electrons) is reflected on or transmitted through a sample. The periodic arrangement of atoms in the sample act as a grating and the radiation interferes constructively only at specific angles, corresponding to the orientations and distances of the atomic planes. The resulting intensity peaks form a diffraction pattern that is recorded by a detector. For *powder X-ray diffraction* the grains, or nanoparticles, in the powder are arranged randomly. Therefore there will not be distinctive spots in the diffraction pattern as there is for single crystalline samples. Instead, the pattern will consist of diffraction rings that can be transformed into a spectrum displaying the intensity as a function of the angle, as is shown in Figure 2.3.

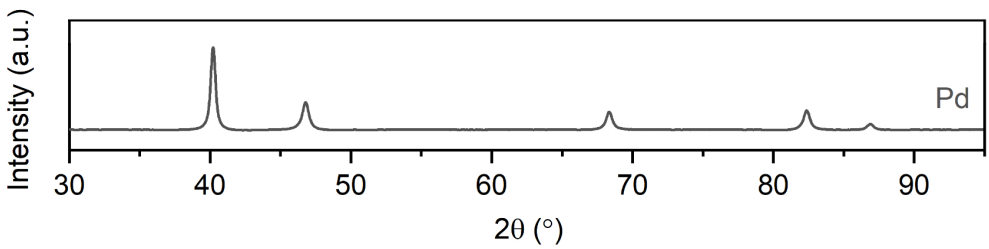

Figure 2.3: Powder X-ray diffraction pattern of Pd nanoparticles with an *fcc* crystal structure.

Chapter 3

Engineered aerosol-generated nanoparticles

Aerosol particles are nano- and micro-sized, liquid or solid, particles suspended in a gas. They are constantly generated around us, from the trees and the oceans, as well as from industries and traffic. NPs can also be generated for a specific purpose, e.g., for sensors [39], printed electronics [40], biomedical applications [41], or catalysts [42]. In order to engineer the NPs for a specific application, control over the properties, such as the material, size, and crystallinity, is necessary. This control is particularly important for the application of catalysis, as the catalytic performance is highly sensitive to the surface structure.

When using aerosol methods to generate particles, the particles are suspended in a gas, which makes it possible to manipulate the particle size, shape and crystallinity before deposition onto a suitable support. In the methods discussed below the generated particles have a size range of about 1-100 nm, i.e., *nanoparticles* (NPs). For these methods the source material is a piece of metal (shape depending on method) that is vaporized, followed by nucleation and growth of NPs by condensation and coalescence.

3.1 Aerosol methods for nanoparticle generation

Aerosol methods for NP generation hold many advantages over the more traditional chemical methods. An important advantage, in particular for the purpose of using the NPs in catalysis, is the absence of reduction agents and stabilizing

agents which might be toxic for the catalyst. In addition, aerosol generation methods are typically continuous, making them suitable for scaling up [43]. There are many different methods for producing aerosol NPs, e.g. laser ablation [15], flame spray pyrolysis [44, 45], electrospray [46], magneto-sputtering [47, 48], thermal evaporation [17, 49], and spark ablation [18, 20]. In the work presented in this thesis the latter two has been used, and their working principles are covered in this section. These methods are both based on vaporization of a metal or semiconductor, followed by rapid cooling by a carrier gas resulting in nucleation and growth of NPs by condensation and aggregation.

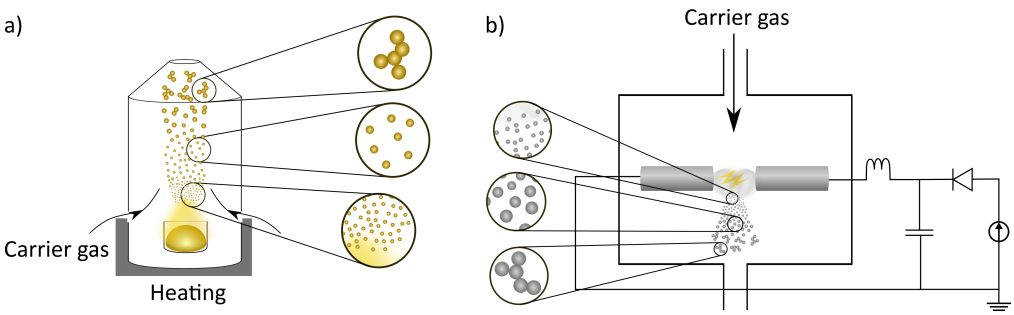

Figure 3.1: Two aerosol methods for generating NPs. a) Evaporation/Condensation, where a metal is heated in a high-temperature furnace to generate a vapor that condenses and coalesces into NPs. b) Spark discharge generator that utilizes a discharge circuit to generate discharged between two electrodes to generate the vapor.

3.1.1 Evaporation/Condensation

The method evaporation/condensation (E/C) relies on thermal evaporation of the material in a high temperature furnace. A piece of the material is placed in a crucible and heated to the temperature required for vaporization. An inert carrier gas transports the vapor away from the heated region, and the rapid cooling causes supersaturation of the metal vapor, resulting in nucleation into atomic clusters that grows into NPs. The NPs will grow as they collide and coalesce until they reach a critical diameter at which the particles start to stick together by van der Waals force to form agglomerate particles [50, 51]. This process is illustrated in Figure 3.1 a). The size distribution of the generated NPs will depend on the partial pressure of metal vapor which, in turn, depends on the temperature of the high temperature furnace. This dependence was studied for gold NP formation by Magnusson *et al.* [17] and in the resulting graph, shown in Figure 3.2, the mode diameter shift with temperature is demonstrated; from sub-10 nm particles for temperatures in the range of 1400–1450 °C to around 30 nm for a temperature of 1650 °C. As the temperature increases, so does the number concentration, making it possible to extract even larger particles with the use

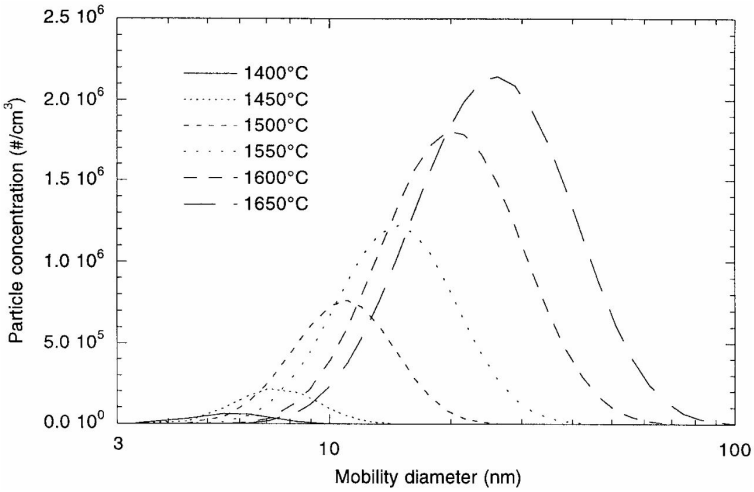

Figure 3.2: Temperature dependence of particle concentration and size distribution. Image retrieved from Magnusson *et al.* [17].

of a differential mobility analyser, which is described below (section 3.1.3). The E/C method can be used for a wide range of metals, although, the tool used in the work described in this thesis operates for gold only and is mostly used to generate seed particles for seed-assisted nanowire growth, which is described further in Chapter 4.

3.1.2 Spark discharge generator

The spark discharge generator (SDG) is based on spark ablation, a highly versatile and scalable method for generating mono-, bi-, or even multimetallic NPs of any non-insulating material [43, 52, 18, 53–56]. The SDG has a simple design with a pair of feedstock electrodes connected in an RLC circuit and positioned in a housing with an inlet for the carrier gas and and outlet for the carrier gas and particles, as illustrated in Figure 3.1 b). The vapor is ablated from the electrode pair by spark discharges. The carrier gas flushes the vapor away from the electrode gap and the rapid cooling results in very high supersaturation and spontaneous condensation of the vapor, followed by growth by coalescence and, finally, agglomeration. Since the vapor is ablated from the electrodes, the electrode materials are chosen based on the target NP material and, since the electrodes can be composed of basically any non-insulating material, including mixtures and alloys, the method provide an immense versatility in terms of chemical composition. Multi-metallic NPs can be generated either by using

electrodes of different materials, or by using pre-alloyed electrodes, consisting of the desired mixture. Similar to the E/C, the SDG operates at atmospheric pressures, making it compatible with common tools for size-selection and thermal manipulation.

An electric discharge results in a certain mass of ablated material. The ablated mass depends both on the circuit settings, which will affect the energy of the spark, E_s, and on material dependent properties which will affect the fraction of the spark energy that goes towards ablating material, and on how much material is ablated with that fraction of the energy. The spark energy, given by Equation 3.1, depends on the capacitance, C, and the discharge voltage, V_d [18].

$$E_s = \frac{1}{2} C V_d^2 \tag{3.1}$$

The proportion between energy input and the ablated mass from the electrode is referred to as the ablatability and is material dependent [20]. It depends on the melting and boiling temperature, T_m and T_b, the specific heat capacity, c_p, the thermal conductivity, k, and melting and evaporation enthalpies, H_m and H_v. This is due to the energy losses during the spark discharges by radiation as light or as heat convection in the surrounding gas, by absorption as latent heat in the electrode material and by conduction along the electrode by metallic thermal conduction. These dependencies were investigated by Llewellyn-Jones *et al.*, who arrived at the balance equation given by Equation 3.2 [57].

$$\begin{aligned} \alpha E_s - \pi r^2 \sigma_s \tau T_b^4 - 2\pi r \tau k (T_b - T) \\ = \Delta m [c_{ps}(T_m - T) + c_{pl}(T_b - T_m) + H_m + H_v] \end{aligned} \tag{3.2}$$

The left side of Equation 3.2 describes the distribution of the energy from the spark, where αE_s is the fraction of the energy transferred to the electrode (the rest is dissipated in the plasma). The energy losses by radiation and heat dissipation through the electrodes are considered by the second and third term, where r is the radius of the spot from which the material is ablated (the "hot spot"), σ_s is the Stefan-Boltzmann constant, τ is the duration of the spark, and T is the temperature at the hot spot. The right hand side describes how much mass is ablated with that energy.

The ablatability, C_{mat}, of different materials is important when synthesizing bimetallic NPs using electrodes o different materials. Several attempts have been made to make predictive models based on Equation 3.2. For example,

Feng *et al.* [43] arrived at a linear relation between ablated mass and the energy of the spark, E, above a threshold value, E_0, by:

$$\Delta m = \alpha C_{mat}(E - E_0) \tag{3.3}$$

In summary, the circuit setting and material properties determine the ablated mass per spark and the spark frequency. This affects the vapor pressure in the gas and the resulting particle size-distribution. As an example, a lower discharge voltage (which can be achieved by a smaller electrode gap) results in a decreased energy per spark, and a lower ablated mass per spark. The size distribution of the generated NPs will thus be shifted towards smaller sizes, although with a lower total particle concentration.

3.1.3 Compaction, size-selection, and deposition

One of the great advantages with the E/C and the SDG is their compatibility with common aerosol tools for manipulation, filtering, counting, and deposition. The set-up used in this work is shown schematically in Figure 3.3 and is described in several publications [58, 59]. After generation in the E/C or the SDG, the NPs pass through a β emitting Ni^{63} neutralizer that provide the NPs with a known charge distribution [60]. The NPs need to be charged for the size-selection and deposition techniques used in this set-up.

The NPs are size-selected using a *differential mobility analyzer* (DMA), a standard tool for classifying charged aerosol NPs based on their electrical mobility, which is related to their mobility diameter [61]. The mobility diameter is the diameter of a spherical particle with the same mobility, defined as the particle velocity produced by a unit external force, as the particle in question [62]. The DMA is useful, not only to select particles with a narrow distribution around

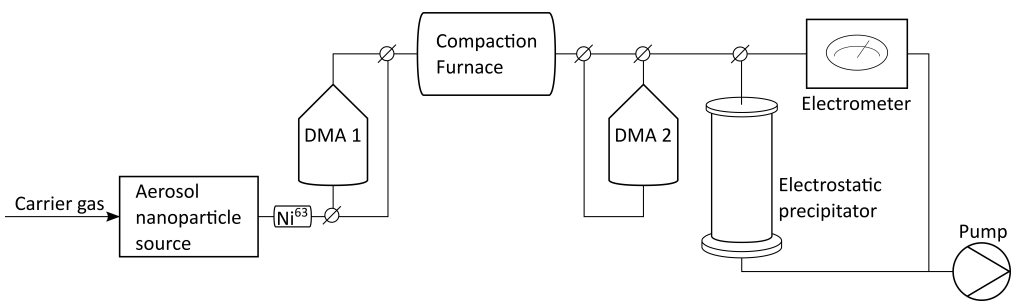

Figure 3.3: Schematics of the aerosol system used for the work described in this thesis.

a specific size, but also for analysis of an unknown size-distribution. A major drawback of the method is the large particle losses that result from passing the aerosol through a DMA, not only of particles with the wrong size, but also of the particles with the target size but with with the wrong charge. However, an important advantage of the DMA is that the particles remain airborne during the size-selection, which is necessary for further manipulation and deposition on the target support.

The aerosol generated in the E/C or SDG consists of agglomerate particles. In order to reshape and compact the agglomerates into spherical, single crystalline particles, they are transported through a tube furnace for *compaction* [17]. As can be seen in Figure 3.4, the compaction begins already at close to ambient temperatures and complete compaction is achieved well below the melting temperature. The compaction temperature, the temperature required to reach full compaction, is material dependent and is related to the vapor pressure of the material, which is size-dependent on the nanoscale, and thus, the compaction temperature is also size-dependent [50]. For easily oxidized materials, a higher oxidation state typically results in significantly higher compaction temperatures. The oxidation can be avoided by by mixing small amount of hydrogen (5 %) in the carrier gas [21].

When the particles has reached the target size and morphology, the charged particles can either be directed to an *electrometer* that counts particles by measuring the current from the charged particles. Alternatively, the particles can be deposited by an *electrostatic precipitator* (ESP). The ESP collects the charged

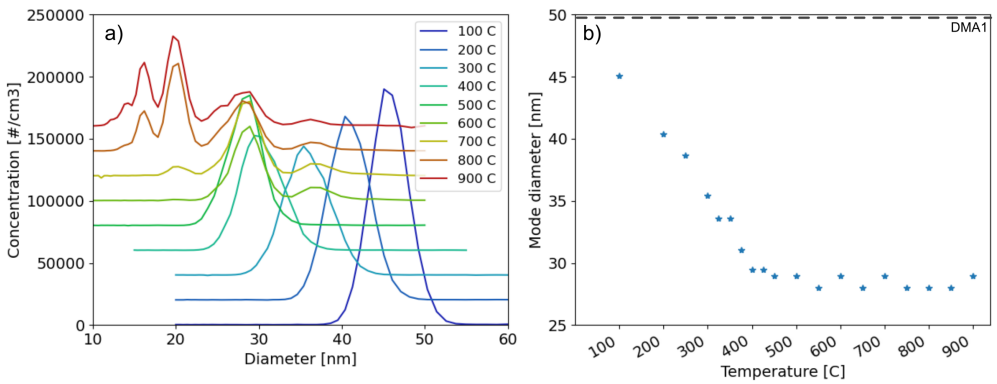

Figure 3.4: a) Scans showing the size distribution of palladium NPs for different compaction temperatures, as measured by scanning DMA2 while keeping DMA1 set to 50 nm. For temperatures $> 700C^{\circ}$, thermal charging occurs, resulting in an increase in multiply charged particles, which is observed as particles with apparently lower diameters. b) The mode diameters for different compaction temperatures, showing the shift in mobility diameter as the NPs are compacted.

NPs in the aerosol onto a stage onto which a voltage is applied [63]. The spot size formed by the deposited NPs can be controlled by the voltage applied on the stage, which is typically a few kilovolts. Preger *et al.* showed that the concentration profile has a top-hat shape, meaning that the NP concentration is constant over the spot size and rapidly drops to zero at a radius, which is determined by the gas flow rate, Q, the distance from the inlet to the deposition plate, h, the applied electrical potential to the plate, φ, and the electrical mobility of the NPs, Z (Equation 3.4) [64].

$$d_{spot} = \kappa \frac{Qh}{\varphi Z} \tag{3.4}$$

One of the large advantages with deposition in ESP, is the immense flexibility of the support, as the support material does not have a large impact on the deposition. However, differences in electrical resistance as well as sharp edges can lead to local build-up in charges causing deflection of the NPs as they are being deposited. This can be utilized, e.g., in order to achieve three-dimensional printing of nanostructures [65].

3.2 Bimetallic nanoparticle generation by spark ablation

Bimetallic NPs have emerged as a fascinating class of nanomaterials with unique properties and versatile applications in various fields, ranging from catalysis and sensing to biomedicine and electronics [66–69]. Among the various synthesis methods available for making bimetallic NPs, spark ablation has gained significant attention due to its ability to produce NPs with control over composition, size, and structure. However, in order to control the composition of the bimetallic NPs, one needs to understand the material-dependent and -independent factors that affect the ablation of the material from the electrodes. Over the past 15 years, several relevant studies have been published on this matter [52–54, 70, 56, 71].

Byeon *et al.* [52] showed that, for monometallic NPs, the rate at which particles are generated follows a distinct order: Ag > Pd > Pt > Au, related to the ionization energy of the materials. Moving beyond monometallic NPs, Tabrizi *et al.* [53] explored effective mixing in bimetallic systems using alloyed and pure electrodes. They successfully synthesized Au-Pd and Ag-Pd NPs using pure electrodes and they found that more material was ablated from the cathode electrode, due to the higher mass of the ions compared to the electrons, carrying

more kinetic energy that could contribute to ablating material. Notably, in the same publication the authors reported that the NPs generated with alloyed electrodes had a composition that reflected the composition of the electrode, despite differences in the vapor pressures of the materials. Tabrizi *et al.* [54] extended the exploration of mixed NPs to metals that are immiscible in the bulk state.

Interestingly, spark ablation enabled the creation of crystalline phases that do not exist on the macroscale. For instance, Au-Cu and Au-Pt formed mixed crystalline phases, which do not exist in the bulk, demonstrating the potential of spark ablation to engineer nanoscale structures with unique properties. Although Cu-W did not exhibit macroscale mixing, successful mixing was achieved at the nanoscale, further expanding the capabilities of spark ablation. This could be explained by the results by Xiong *et al.* [70] who studied the thermodynamics of bimetallic particle formation and found a relationship between particle size and the formation enthalpy and Gibbs free energy of formation. As particle size decreased below a critical size, they found that both formation enthalpies and Gibbs free energies exhibited a decline, leading to thermodynamically favourable conditions for formation of otherwise immiscible materials.

Feng *et al.* [56] contributed to the field by developing a model (based on Equation 3.3) that takes into account both material-dependent and circuit-dependent factors to explain and control the composition of mixed NPs synthesized from electrodes of different materials. The authors concluded the following formula for the fraction of material contribution from the cathode electrode:

$$\varphi_C = \frac{1}{1 + \frac{C_A}{k \cdot C_C}} \tag{3.5}$$

where C_A and C_C are calculated from Equation 3.2 for the anode and cathode material, respectively, and k is the asymmetry of the current waveform of the spark discharges. The model provides a comprehensive understanding of the factors governing NP composition, enabling increased control over the synthesis process. This model has, however, been criticised for only considering the current waveform when estimating the energy delivered to the electrodes and the mixing model was extended by Kohut *et al.* to include the voltage fall over the anodic and cathodic electrodes to better predict the experimental results [71]. The authors further proposed that control of the circuit resistance could lead to full range tuning, although, their demonstration only showed small shifts in particle composition. They suggested that exploring more electrode configurations might be the key to achieving the desired control.

The studies reviewed here collectively demonstrate the capabilities of spark ablation in generating bimetallic NPs with tailored properties. By understanding the influence of electrode materials, thermodynamics, and mass transport during the synthesis process, researchers aim to optimize the NP generation for specific applications. The ability to synthesize mixed NPs of immiscible metals to create unique nanoscale crystalline phases would open up exciting possibilities for engineering materials with unprecedented properties. In the pursuit of achieving full compositional range tuning of bimetallic NPs, the field still faces some challenges. In our study, we have taken this challenge head-on and present an approach that involves various electrode configurations.

3.2.1 Compositional tuning of Pd-Cu nanoparticles

In this section, the results from Paper I are summarized.

As established in the previous section, bimetallic NPs are promising components for functional materials. Compositional control is a vital part for optimization of these particles for tailored properties and performance. This section aims to delve into the details of progress on compositional tuning of Pd-Cu bimet-

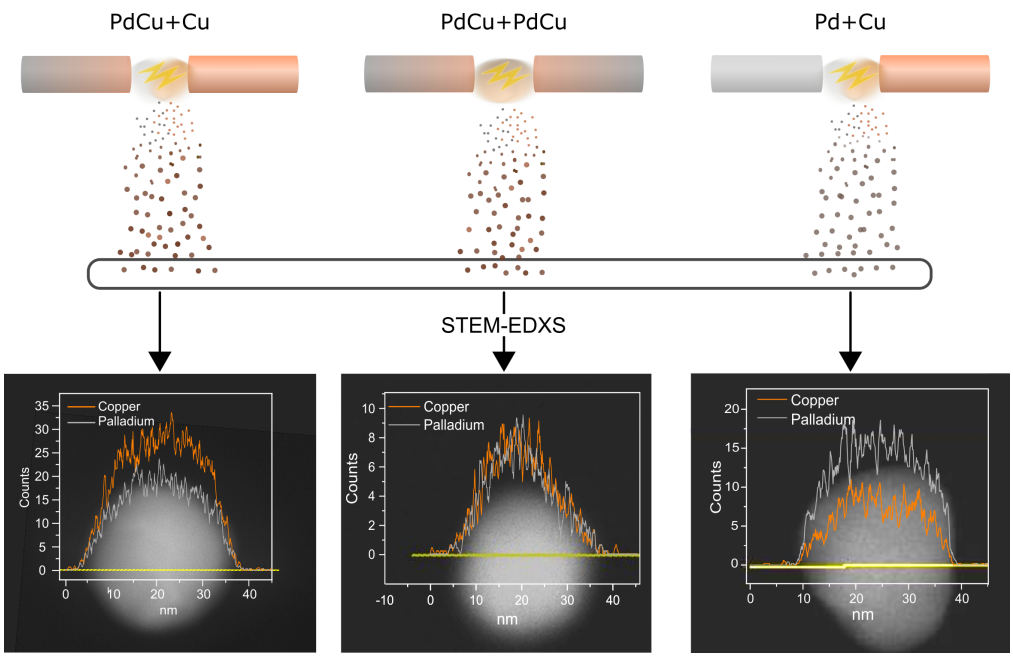

Figure 3.5: STEM micrographs with overlaying STEM-EDXS line scans, showing the composition across the particles generated with different electrode configurations, shown above as "anode+cathode".

allic NPs using spark ablation. The investigation encompasses the analysis of chemical composition at both ensemble and individual NP levels, exploring the implications particularly for catalytic applications.

The study utilized time-resolved X-ray fluorescence (XRF) measurements at the ensemble level to determine the chemical composition of the synthesized NPs. By employing different electrode pairs, including pure and alloyed electrodes, we successfully demonstrated the ability to tune the composition within a range of approximately 80:20 at. % to 40:60 at. % (Pd:Cu). Transmission electron microscopy energy dispersive X-ray spectroscopy (TEM-EDXS) analysis of individual NPs confirmed that the deviation in composition between individual NPs was negligible. Scanning TEM-EDXS line scans further revealed the well-mixing of Pd and Cu within individual NPs, indicating a homogeneous distribution of the two metals (see Figure 3.5).

To gain insights into the outermost atomic layers, which are crucial for catalytic applications, X-ray photoelectron spectroscopy (XPS) and X-ray absorption spectroscopy (XAS) were employed on the NPs synthesized using alloyed electrodes. The analysis, based on XPS performed with different photon energies, showed that the composition of the outermost atomic layers was consistent with that of the deeper layers, suggesting a uniform composition throughout the NPs. This finding is significant since it ensures the surface composition accurately reflects the overall NP composition, reinforcing the potential catalytic efficacy of the bimetallic NPs.

Time-resolved XRF measurements provided valuable insights into the dynamics of composition changes during the ablation process. The NPs generated using a Pd anode and a Cu cathode exhibited a shift in composition over time. It is not trivial to explain this result, since many different factors could contribute to this effect. A vapor cloud is formed between the electrodes as material is ab-

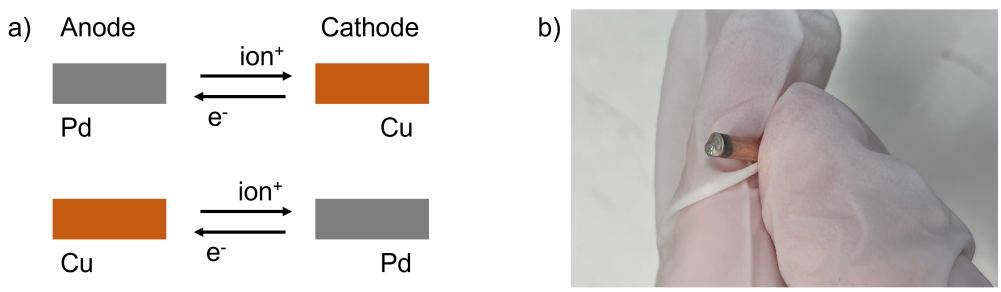

Figure 3.6: a) Schematic illustrating the ion and electron exchange during a spark discharge. b) Copper electrode after being used as a cathode together with a palladium anode, showing the re-deposition of palladium.

lated between them. This vapor can diffuse and condensate onto the electrodes. This effect could be diminished by increasing the electrode distance. There are also a large amount of ions in this vapor cloud, which could be attracted to and deposited onto the electrode with opposite charge. Finally, there is a direct transfer of ions and electrons between the electrodes during the spark discharge, see Figure 3.6. Since the initially anodic electrode is positive for a longer duration in total, there will be more ions transferred from an electrode if it is initially anodic, although, the ablatability is also an important contributing factor. This finding highlights the significance of time-resolved composition measurements and emphasizes the influence of electrode configuration on NP composition. To minimize such composition changes, the use of pre-alloyed electrodes is recommended when feasible.

This study successfully demonstrated the ability to tune the composition of Pd-Cu bimetallic NPs using spark ablation. The comprehensive analysis of chemical composition, both at the ensemble and individual NP levels, revealed the homogeneity and well-mixing of Pd and Cu within the NPs. The investigation of the outermost atomic layers ensured that the surface composition accurately represented the overall composition, crucial for catalytic applications. The expansion of the electrode set and the exploration of time-resolved composition changes further enhanced our understanding of compositional tuning. These findings provide valuable insights for the development of efficient and cost-effective bimetallic catalysts and lay the foundation for future studies on other binary metal systems.

Chapter 4

Epitaxial growth of gallium phosphide nanowires

Compound semiconductor nanowires (NWs) are versatile building blocks with an array of applications spanning diverse fields, e.g., advanced solar cells [25], high-performance photodetectors [72], and cutting-edge transistors [73]. These nanostructures, characterized by their high aspect ratios, large surface area, and a morphology that can be controlled with high precision, make them interesting candidates for support structures in model catalysts.

NWs can be synthesized either by a top-down or a bottom-up approach. Top-down synthesis typically incorporates some kind of milling [74] or etching [75] from a bulk material, to carve out the target structure. Bottom-up means that the structures are self-assembled, typically by epitaxial growth such as molecular beam epitaxy (MBE) [76] or metal-organic vapor phase epitaxy (MOVPE) [77].

In this work we use close-packed tapered gallium phosphide (GaP) NWs as supports for catalytic NPs. GaP NWs has previously been used in several biological applications, such as directed drug delivery and diagnostics, and have demonstrated chemical stability [78, 79]. The design was optimized with two aspects in mind, the first being chemical and mechanical stability, and the other to make the catalytic NPs accessible to the reactants. The catalytic application is presented in Chapter 6.

4.1 Metal-organic vapor phase epitaxy

MOVPE is one of the most common methods for compound semiconductor NW growth due to its versatility and precision. The process is based on the injection of gaseous precursors in an inert carrier gas into a reactor with a laminar flow. If the conditions are favourable, which can be controlled by growth parameters, the precursors react on the substrate, resulting in growth of epitaxial layers, i.e., layers that adopt the crystal structure of the underlying layer [80]. Within MOVPE, numerous growth mechanisms are possible, including:

- selective-area growth, where the surface is masked except for in specific areas where the epitaxial growth is intended [81];
- self-nucleating growth, where the growth is catalyzed using the same, or one of the same, material as the grown material [82];
- aerotaxy, a substrate-free method operating at atmospheric pressure and associated with high growth rates. The growth occurs in the gas-phase and is catalyzed by aerosol metal particles [83, 84]; and
- particle-assisted growth [85, 86], which is the mechanism used in the research presented in this thesis.

This chapter includes an overview of the key factors in MOVPE growth, particle assisted growth, beginning with an illustration of its fundamental principles and on the different growth regimes. Following this background, is a presentation of experimental results of the growth of tapered close-packed NWs and of the Pd seeded NWs and branched growth.

4.1.1 Key factors in MOVPE

The process of MOVPE growth is highly complex and includes thermodynamic, kinetic, and mass-transport components, as well as transitions over multiple phases. However, due to tremendous efforts over the last decades, the basic processes are fairly well understood [87–89].

Thermodynamics determines the driving forces in epitaxial growth. Any closed system has a thermodynamic equilibrium associated with it, which describes the state of that system given enough time. In the equilibrium state, the Gibbs free energy per mole is minimized, and this sets the limits for the maximum growth rate, resulting alloy composition, and crystal structure. Thermodynamics can

thus be used to understand the relationship between the various phases in a system, and use that to control the driving forces for epitaxial growth.

However, MOVPE is a non-equilibrium process, and the steps involved to move towards equilibrium can be described by the kinetics of the chemical reactions and of the mass-transport. Considering the kinetics, the rate constant, k, of the chemical reactions for the pyrolysis of the precursors can be expressed by the Arrhenius equation:

$$k = Ae^{-E_a/k_B T}$$

where A is called the preexponential factor, E_a is the activation energy, k_b is Boltamann's constant, and T it the temperature. The kinetics parameters are closely related to the thermodynamic properties of the system, e.g., the difference in activation energy of the forward and reverse reaction is equal to the difference in the thermodynamic enthalply of the two states; and at equilibrium the rates of the forward and reverse reaction are equal.

For the mass-transport in a MOVPE reactor, the macroscopic gas flow is governed by hydrodynamic effects, which describes how fluids interact with each other and with solid surfaces, and includes principles governing fluid flow behavior. However, to understand the growth rate when limited by mass-transport, one need to consider the migration of precursors close to the surface. For this purpose, the boundary layer-model is commonly used, in which the mass-transport to the surface occurs by diffusion [90]. This process is close to temperature independent.

When studying epitaxial growth, it is possible to gain knowledge about the system by testing how the growth rate depends on different factors, including: precursor partial pressure, which for an ideal gas is the total pressure multiplied by the molar fraction of the precursor molecule; temperature, which affects both the equilibrium state and the kinetics of the growth; and flow rate, which is especially important when the growth is limited by the mass-transport. As an example, the growth limiting process can be determined by studying the temperature dependence of the growth rate. If the growth rate increases with temperature, the growth is kinetically limited; if the growth rate decreases with temperature, the growth is thermodynamically limited; and if the growth rate is independent of temperature, the growth is mass-transport limited, as gas-phase diffusion is nearly temperature independent [90].

4.1.2 Particle-assisted growth

In order to further control the epitaxial growth, one can rely on particle-assisted growth, which enable growth in one direction, resulting in NWs. It was first developed by Wagner *et al.* in the 1960s [91], with the first bottom-up growth of what was at the time referred to as "whiskers". In particle-assisted growth, the seed particles act as a collector of the precursors and facilitates growth at the interface between the particle and the substrate [92].

The mechanisms involved in particle-assisted growth include adsorption of precursor species, either directly onto the seed particle, or on the substrate or NW side-walls, adatom migration to and through the seed particle by diffusion, followed by epitaxial growth at the particle-NW interface. For the typical condition, where the seed-particle is in a liquid phase during growth, this growth mechanism is referred to as vapor-liquid solid (VLS) growth, which refers to the phases involved during the growth. An illustration of these processes are shown in the inset in Figure 4.1, along with the MOVPE system EpiQuip used for this work.

In parallel, a competing process of direct surface growth, or vapor-solid (VS) growth, on the substrate or the NW side-walls, can occur. If growth conditions allow for both VLS and VS growth, the resulting NWs will have a tapered

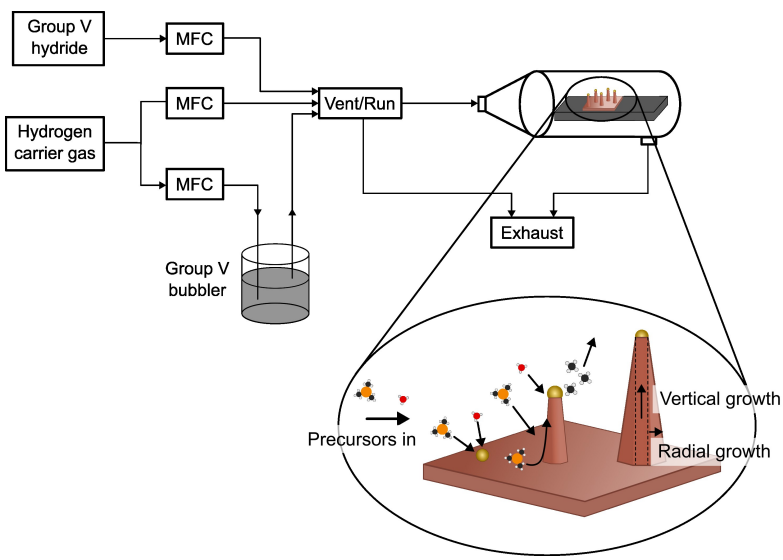

Figure 4.1: Schematics of the MOVPE system EpiQuip and the processes during particle-assisted growth, illustrating the adsorption, diffusion, and desorption of species onto, along, and from the support as well as the growth evolution of the NWs.

shape, where the base is wider than the tip of the NW. This effect is normally not desired, as the radial growth generally have poorer crystal quality compared to the axial growth. Therefore, research has mainly been focused towards suppressing the radial growth [23, 93–96]. Since the seed particle acts as a catalyst for the growth, the seeded growth can take place also at temperatures at which VS growth does not occur, resulting in NWs with the same diameter along the entire length.

So far, we have assumed a liquid seed particle during growth. However, it is possible to achieve growth also with a solid seed particle, which is referred to a vapor-solid-solid (VSS) growth. The phase of the seed particle has been found to have a large impact on the resulting growth, where VLS is generally related to higher growth rates in the vertical direction and high axial control [97–99], while VSS growth tend to result in unstable growth direction (kinking) [100, 101]. Because of the difference in growth behaviors between the VLS and VSS mode, it is important to consider the melting point of the seed particle when choosing the growth parameters. The melting point of the seed particle depends on the size of the NPs, as well as their composition, as new phases will form in the seed particle when the precursors are introduced in the reactor. These phases can be controlled by the partial pressures of the group III and group V precursors.

4.2 Growth of tapered gallium phosphide nanowires

The purpose of the NWs developed in this work was to be used as support structures for catalytic NPs to elevate the NPs from the support surface to increase their accessibility to reactants. In order to maximize the amount of reaction solution surrounding the NPs on the NW tips, an initial design with narrow (∼10 nm diameter) NWs was tested, as the one shown in Figure 4.2 a). However, when these structures were immersed into a liquid solution, they did

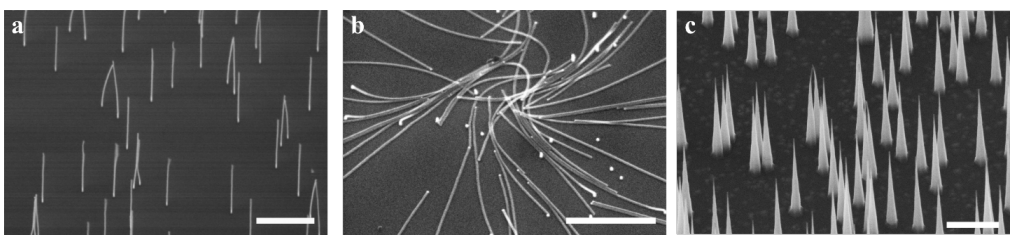

Figure 4.2: NWs before (a) and after (b) immersion and retrieval from liquid solution (acetonitrile). c) Tapered NWs for enhanced mechanical stability. Scale bar is 0.5 µm.

not have the mechanical stability necessary to withstand the forces imposed on them by the liquid and they would break off from the surface, see Figure 4.2 b). By simply increasing the diameter of the entire NWs would lead to less accessible solution or less surface area (if the number density would be decreased), which is not desired in this case. As an alternative, a tapered design was proposed, as imaged in Figure 4.2 c). This, typically unwanted, feature would here be useful as it provides mechanical stability, while keeping the volume surrounding the tips free and accessible to reactants.

For the purpose of using these NW structure as supports in a model catalyst, it was not only important to find the optimized design, but also to achieve the control over the NW growth to enable independent tuning of the NW dimensions. This would provide the necessary tools to study the influence of the support design on the catalytic response. Therefore, it was important to gain further understanding of the growth of close-packed, tapered NWs.

4.2.1 Controlling nanowire dimensions: gold-seeded growth

Gold (Au) as a seed particle material dominates the literature on particle-assisted growth. This is partly because of historical reasons, it was used early on and thus became well-studied [102], although, more importantly, Au has properties that makes it suitable for VLS growth. For example, Au has the ability to form low-temperature alloys, and many precursor materials used in growth is soluble in Au [103]. Because of the flexibility of Au-seeded growth, Au was chosen as the seed particle material for the initial NW development presented in this work. The focus of the development was to find the parameters to control the length, width, and tapering of close-packed NWs. The high concentration of NWs increases the competition for the precursors, and thus, the significance of mass transport of precursors to the substrate and the seed particle-NW interface, where the growth takes place.

General procedure for tapered nanowire growth

The samples were prepared for NW growth by deposition of seed particles with a diameter of 10 nm, generated by E/C and deposited electrostatically, by methods described in Chapter 3. The electrostatic deposition results in randomly distributed NPs and the average concentration was 40 μm^{-2}. The NW growth was done in an EpiQuip MOVPE. After placed in the reactor, the sample was annealed at 600 °C for 10 minutes. The annealing step is done to remove the

surface oxide layer on the substrate and to initialize the nucleation of the crystal growth. During the annealing step, there is a partial pressure of phosphine (PH_3) in the gas flow to avoid decomposition of the surface. After the annealing followed a growth step at a temperature of 560 – 600 °C, for which trimetyl gallium (TMGa) was introduced along with the PH_3. The growth time varied from 1 to 13 minutes, depending on the growth parameters used and on the target NW shape. The grown NWs were imaged by SEM and the micrographs were analyzed using ImageJ.

Effect of V/III ratio on nanowire growth morphology

The effect of the V/III ratio on the resulting NW morphology was studied for a range from 50 to 320. The growth temperature was 600 °C and the growth time was 3 minutes for all growths. In Figure 4.3 we see that increasing the V/III ratio resulted in shorter and wider NWs, i.e., more radial growth and less vertical growth. The most significant shift was observed in the range of V/III = 100 − 200. For the seeded growth the gallium is first collected in the seed particle. This shift from more vertical growth to more radial growth can be explained by considering the supersaturation of Ga at the seed particle-NW

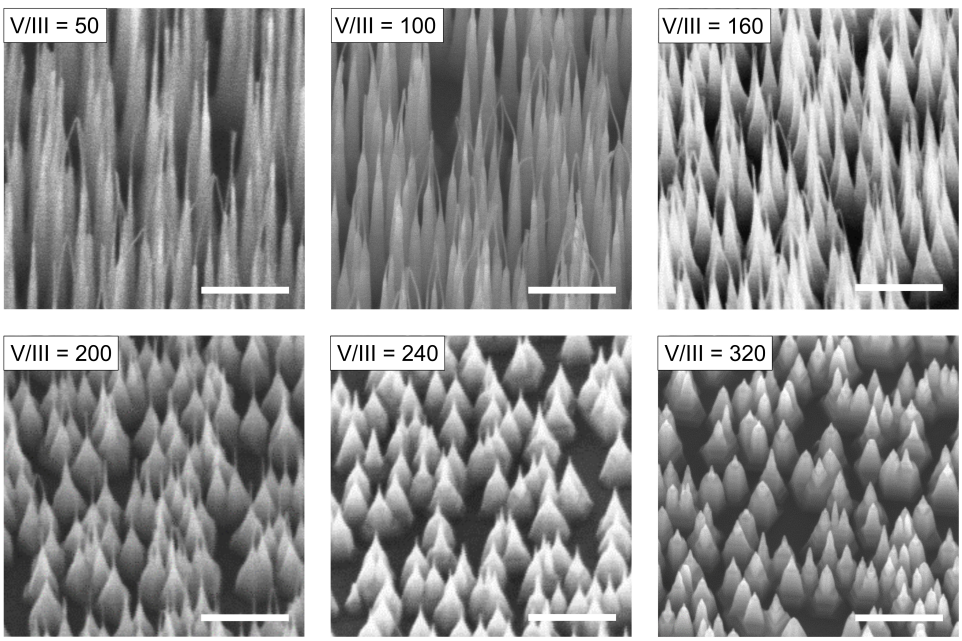

Figure 4.3: NW growth at different V/III ratio, grown at 600 °C, showing a clear shift from high to low aspect ratio as the V/III ratio is increased. Scale bar is 500 nm.

interface, which is the driving force in VLS growth. For the lower V/III ratio, the supersaturation is high, resulting in a higher growth rate (GR). For the higher V/III ratio, the supersaturation is lower, resulting in lower GR. The large excess of PH_3 available for high V/III ratios also increases the probability for the TMGa to react with PH_3 before reaching the Au seed, which would promote radial/VS growth.

Nanowire length and tapering: growth time and temperature effects

The NW length and tapering was studied for different growth times and temperatures. The temperature interval 560–600 °C was chosen since it is the range where both vertical and radial growth generally occurs for GaP, resulting in tapered NWs. The measurements were made *ex situ*, so each data point in Figure 4.4 a-b) comes from different growths.

The resulting NW length for different growth times and growth temperatures are shown in Figure 4.4 a), and the slope of the fitted line can be interpreted as the vertical GR. It can be seen that the vertical GR decreases both with temperature and with time. The decrease in GR with increasing temperature indicate that the growth is thermodynamically limited within this temperature range. This is in agreement with what was observed by Berg *et al.* [93] for growth of GaP NWs. The decrease in vertical GR as growth time increases is not as easily interpreted, although it could be attributed to mass-transport limitations as more material is consumed by the competing radial growth. As growth time increases, the NWs grow longer and there is more surface area available for VS growth.

In Figure 4.4 b), the tapering of the NW is presented for different growth times and growth temperatures. The tapering decreases slightly for higher growth times. This this can be explained by the lower vertical GR, which provides longer time for radial growth in the top part of the NW. This effect can be seen for the NWs shown in Figure 4.4 c) and d), that had been grown under the same conditions for 6 minutes and 7.5 minutes, respectively. For the NW with the longer growth time, the top parts of the NWs are thicker compared to the shorter growth time. The ultra-tin tips could thus be avoided by increasing the growth time to the range where the vertical GR is lower, thus allowing time for radial growth also at the top parts of the NWs. This was important for the stability of the NWs when used in catalytic reaction, as is discussed in Chapter 5.

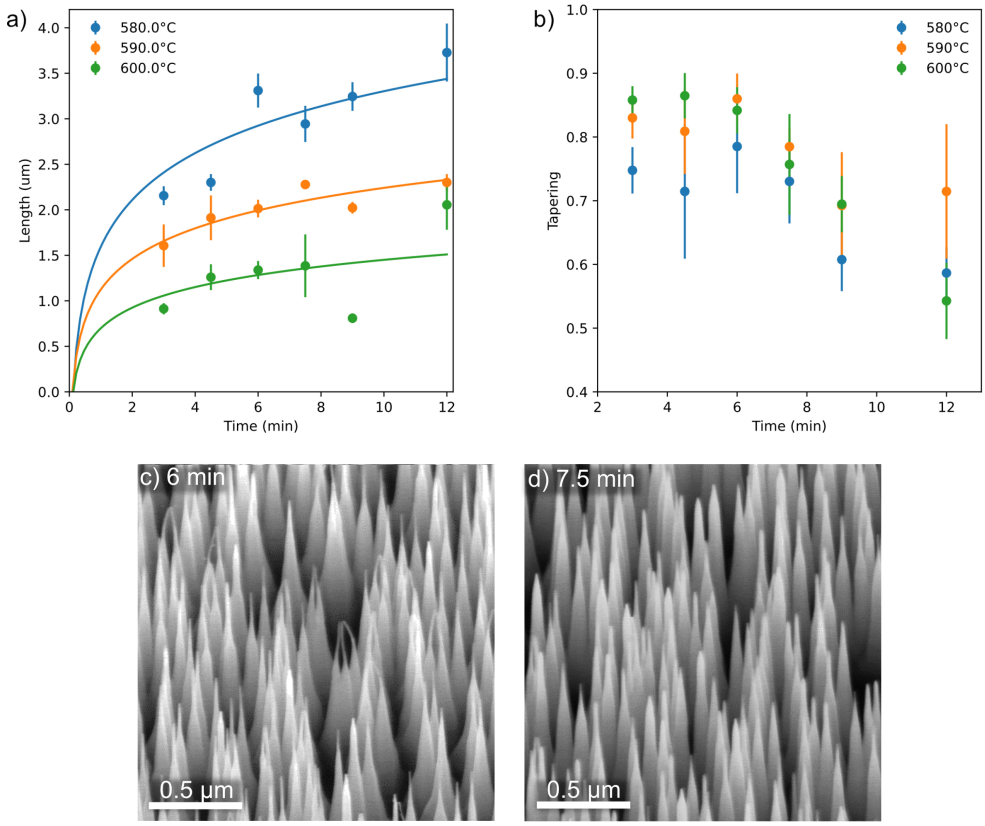

Figure 4.4: Vertical length (a) and tapering (b) of NWs grown with V/III=200, and varying growth times and growth temperatures. SEM images of NWs grown with a growth temperature of 590 °C, V/III=200, and a growth time of a) 6 minutes and b) 7.5 minutes. Showing how the increased thickness of the top part of the NWs, explaining the decreasing in tapering for longer growth times.

4.2.2 Palladium-seeded growth

The work presented in the remainder of this chapters is based on Paper II and covers the growth of GaP NWs and branched nano-trees using palladium (Pd) as the seed material. The focus of this work was to optimize the growth conditions, with the objective to utilize the GaP NWs and nano-trees for catalysis.

Pd was chosen as an alternative seed particle material because it is an effective catalyst for various reactions [104–107]. However, a challenge when replacing Au with Pd is that the same growth conditions can no longer be applied. For example, the Pd-Ga alloy have a higher melting temperature compared to Au-Ga for most compositions, which is clear when studying the equilibrium phase

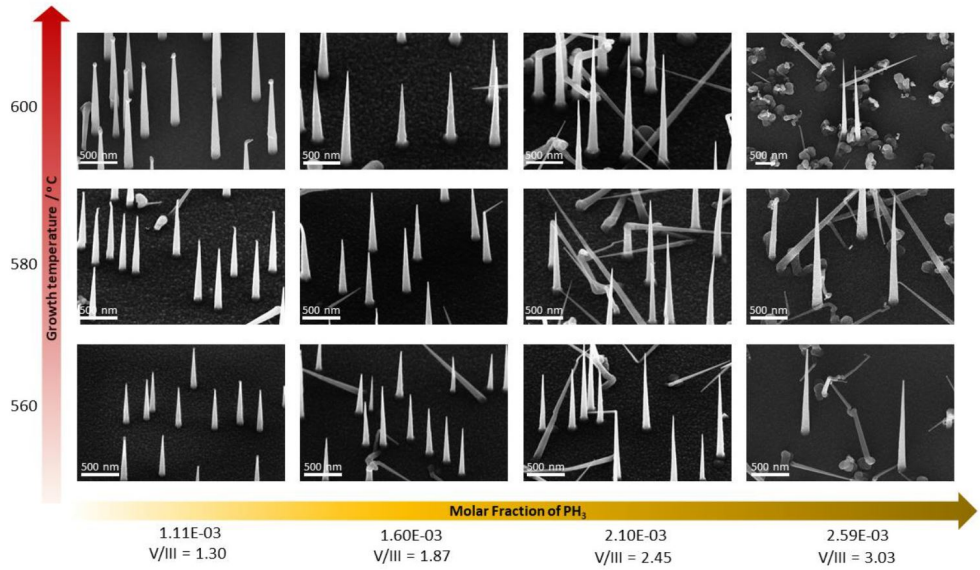

Figure 4.5: SEM images of Pd-seeded GaP NWs, using Pd seed particles with a diameter of 10 nm, at different growth times and V/III ratio. Image retrieved from the Supplementary Information of Paper II.

diagrams [108, 109]. For the Pd-Ga alloy, the Pd concentration needs to be lower than 22 at.% for the alloy to have a melting point below 600 °C.

In order to achieve a higher Ga concentration in the Pd seed particle, the V/III ratio was reduced significantly from what was used for the Au seeded growth. In Figure 4.5 are the growth results from using a V/III ratios of 1.30 – 3.03 (TMGa molar fraction fixed at $8.56 \cdot 10^{-4}$, while the PH_3 molar fraction varied between $1.11 \cdot 10^{-3} - 2.59 \cdot 10^{-3}$) and temperatures of 560 – 600 °C. For the higher V/III ratios there are a lot of kinked NWs and excessive surface growth, which is characteristic for VSS growth (solid seed particle). The highest yield of straight NWs was achieved with a growth temperature of 560 °C and a V/III ratio of 1.30. Surprisingly, a higher growth temperature resulted in a higher fraction of kinked and curly NWs, which indicates non-continuous growth.

At a V/III of 1.30, the limit of the EpiQuip MOVPE was reached. In order to study the effect of further decreasing the V/III, another MOVPE was used, an Aixtron CCS 18313. With this MOVPE it was found that a lower V/III ratio resulted in inflated seed particles (lollipop-shaped NWs). This effect was likely due to a shift in the balance between the precursors, leading to a higher Ga incorporation in the Pd seed particle, combined with insufficient PH_3 available for growth that can consume the Ga in the seed particles.

4.2.3 Branched growth

In order to increase the total surface area of the support, a three-dimensional design was developed with branches grown from Pd seed particles deposited onto the core NWs.

The core NWs were grown using the optimized conditions presented in the previous section, with a V/III ratio of 1.30 and a temperature of 560 °C. Pd NPs were deposited onto the core NWs, using the same procedure as for the core growth, although with a higher NP particle concentration, ranging from 100 – 1000 μm^{-2}. The SEM images in Figure 4.6 show the Pd NP-decorated core NWs (a-d) and the resulting nanotrees (e-h), grown with the different NP concentrations and using the same growth conditions as for the growth of the core NWs but with a growth time of 10 s. Since the core NWs were not very close-packed, only a small fraction of the deposited seed particles were collected by the NWs, and could contribute to the branch growth.

It was observed that the branch growth had a GR of about 0.5 µm/min, which can be compared to the GR of the core NWs of about 0.9 µm/min. The low GR of the branches indicate competition of the precursor material among the seed particles, pushing the growth into the mass-transport limited regime. A similar effect was observed when comparing the growth branches for the different NP concentration in Figure 4.6 e-h), where the higher NP concentrations resulted

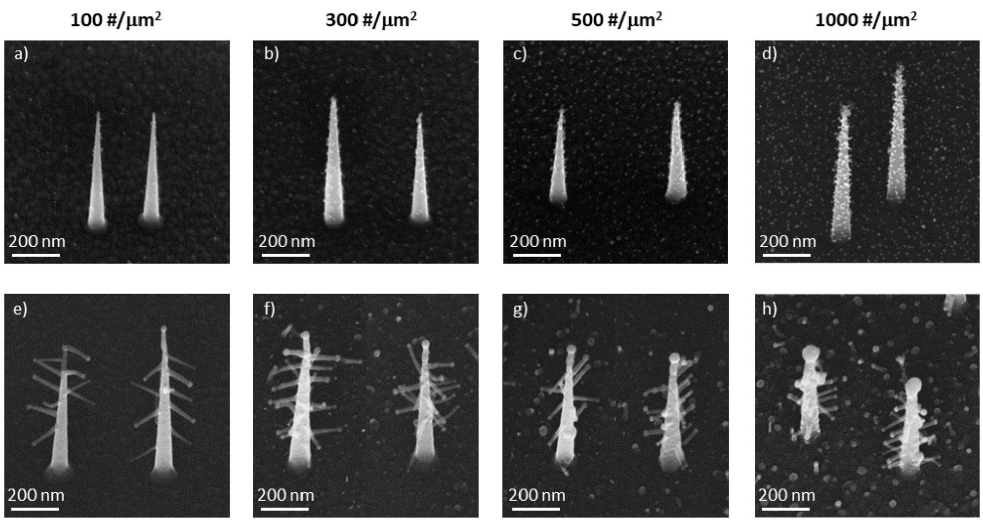

Figure 4.6: a)-d) SEM images of core NWs seeded by 10 nm Pd seed particles and decorated with Pd NPs for branched growth with concentrations of 100, 300, 500, and 1000 μm^{-2} Pd NPs, respectively. e)-h) the resulting nanotrees from the respective cores. Image retrieved from the Supplementary Information of Paper II.

in shorter branches, compared to the lower NP concentrations.

Interestingly, top-view SEM images (see Paper II, Figure 5), display a six-fold symmetry of the grown branches. This symmetry arise from the preferential growth in the three <111>B directions [110]. Due to stacking faults in the core NW, the <111>B direction is rotated 60°, resulting in a six-fold symmetry.

The successful growth of Pd-seeded NWs and nanotrees is highly promising for the application of catalysis. The Pd seed particles are well-attached to the core NWs and branch tips, and thus, no NP migration or clustering is expected. However, it is feasible that the Pd-seed particles have different catalytic properties compared to the as-deposited Pd NPs due to possible Ga or P incorporation in the particles during NW or branch growth. The evaluation of these structures, both in terms of stability and catalytic performance is, however, outside the scope of this thesis.

Chapter 5

Stability of supported aerosol-generated nanoparticles in liquid media

In this chapter the work performed on the stability of supported aerosol-generated NPs in liquid media is presented. The first part of the chapter is based on Paper III and focuses on the stability of particles on planar supports. In the second part of the chapter, the stability associated with the nanowire supports is presented.

5.1 Importance of stability in catalysis

The stability of NPs and their supports is a critical aspect for the successful use of them in liquid environments. Typical stability issues in NP catalysis are NP clustering and sintering, atomic leaching, and poisoning [111]. Coalesce of clustered NPs into larger particles has also been found to deactivate the catalyst [112, 113].

Another effect that can cause issues for the catalyst during exposure to liquids is atomic leaching of the NPs, resulting in single atoms or atomic clusters being released into the solution. These atoms or clusters are often highly catalytically active and might contribute to the catalytic conversion, making it difficult to isolate performance of the solid catalyst [114]. Leaching of catalytic material might also impose issues in regards to the strict regulations that exist on heavy

metals in pharmaceuticals [115]. Finally, maintaining the structural integrity of the catalyst is an important criteria for the ability to re-use the catalyst, which is an aspect that significantly decreases the cost connected with using the catalyst.

Understanding the impact of solvents on the stability of NPs on a support is essential for optimizing their performance and ensuring their reliability. The stability of the support is also relevant when studying the catalytic properties of the supported NP catalysts, here referred to as *NP chips*. Both because the stability of the surface can affect the stability of the NPs, i.e., if the surface is etched it is very likely that the NPs will come off as well, but also because the surface often has an effect on the catalytic activity of the NPs [116, 117].

To identify reaction conditions where the NP chips are stable, a large systematic mapping on the effect of NP chip exposure to different solvents was carried out. This was done for different support and NP materials. In addition, since many reactions require basic or acidic conditions, the effect of changing the pH of the solution was investigated. Finally, the effect of heat treating the NP chips post-deposition, before exposure to the solvent, was tested.

5.2 Stability: planar supports

The stability of aerosol-generated metal NPs on semiconductor or oxide supports was studied as they were exposed to various solvents commonly used for different applications. A systematic approach was developed, for which identical location scanning electron microscopy (IL-SEM) was used in combination with density- and size analysis to comprehensively analyze the stability of the NPs and their supports. The combination of particle and support material plays a crucial role in determining the stability of NPs in different liquid environments. The study elucidates the importance of carefully selecting compatible combinations to withstand specific solvents. For each NP–support system investigated, both protic and aprotic solvent conditions were identified for which both the particle and support demonstrated sufficient stability. The addition of organic acids was found to be well tolerated, while basic additives showed a negative impact on stability in some solvents.

5.2.1 Identical-location SEM

To detect small NP movements that might not be detected by ensemble measurements of the NP size and density analysis, identical location imaging was performed with a scanning electron microscope (Hitachi SU8010). SEM images were acquired of the NP chip in the exact same location before and after treatment in solution. Examples of the results are shown in Figure 5.1. Keep in mind that, in order to resolve the 10-nm sized NPs, high magnification is required. The micrographs in Figure 5.1 display an area of about 1.25 μm^2, meaning that one sample could fit more than 50 million such micrographs, none of them showing the same area. Thus, a reference marking was used in order to navigate on the sample and find the same location. Two fine lines, made with a diamond pen, forming a cross over the sample, were used as markings. An image was acquired in each of the quadrants around the cross.

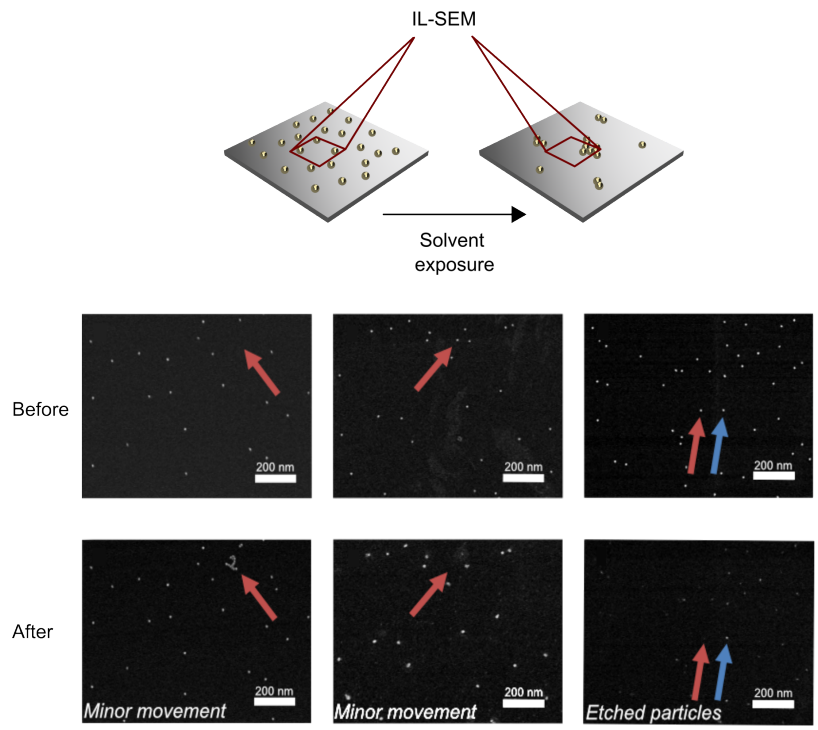

Figure 5.1: Schematic illustrating the principle of IL-SEM and examples of results from solvent exposure with minor NP movement and etched NPs.

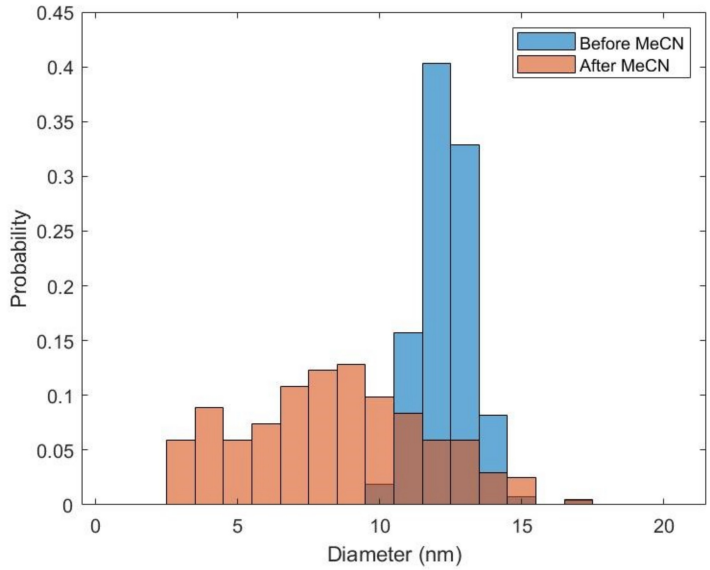

Figure 5.2: Histograms showing size distribution of Au NPs on Si before and after treatment in acetonitrile (room temperature) for 24 hours, showing a clear shift towards smaller NP sizes due to atomic leaching of the NPs. Distributions are based on 268 and 203 particles, respectively.

5.2.2 Size- and density analysis

A weakness of the IL-SEM is that the reference areas were imaged before the treatment, exposing that area, including the NPs, with a scanning 15 kV electron beam, resulting in local heating of the sample [118]. This could have an affect on the NP adhesion to the surface, increasing their stability in solution. In order to control for such an effect, images were acquired in additional areas after the treatment. These areas did not allow us to track single NPs, however, it was possible to track if the NPs were evenly dispersed on the surface or if there had been linking or clustering of the particles. The additional imaged areas were also used for analysing any shift in density or size-distribution of the NPs. Examples of such size-shift, resulting from atomic leaching of the NPs during exposure to acetonitrile (MeCN), one of the tested solvents, are shown in Figure 5.2.

5.2.3 Result summary

The results of our study demonstrate that the choice of solvent has a significant impact on both the NPs and their supports. Commonly used solvents and additives were found to influence the behavior and stability of aerosol-generated

NPs. This observation underscores the critical role of solvent selection in NP applications. The stability of the NP supports was also found to be strongly dependent on the solvent in which they were immersed. Variations in solvent properties, such as polarity and acidity, affected the adhesion of NPs to the support surfaces.

From the results, it was clear that some solvents affected the NPs, e.g., resulting in movements on the support, other solvents affected the support, e.g., by etching of the surface, and some solvents did not affect the NP chips at all. Overall, the NPs were stable in most solvents, but there were some exceptions and noteworthy findings:

- Exposure to water at room temperature and elevated temperature (95 °C): When exposed to water at room temperature, new NPs found in the observed areas on the surface, indicating that particles has migrated over the surface. At 95 °C, the silicon surface became slightly roughened, and the particle size increased, possibly due to gold particle overgrowth with silicon.
- Stability in cell growth media (PBS Buffer): Immersion in phosphate-buffered saline solution (PBS buffer) resulted in salt residues remaining on the surface, preventing imaging and conclusive evaluation of stability.
- NP etching: The NPs were resilient to most organic solvents tested, except for acetonitrile (MeCN), which led to significant etching of the NPs. Triethylamine (Et_3N), a soluble organic base, was well tolerated, while inorganic bases caused severe etching.
- Effect of support materials: Gold NPs on gallium phosphide showed instability in water, causing corrosion. NPs on silicon and alumina both showed good stability. Palladium NPs exhibited different stability compared to gold NPs in some solvents.
- Thermal annealing: Thermal annealing of gold/silicon supports was found to significantly improve NP adhesion and enhance their resilience to water, even at elevated temperatures. This finding suggests that thermal treatment can be a useful strategy for enhancing the stability of supported NPs in solvent-based applications. However, annealing did not enhance resilience to the etching in acetonitrile.

The study on the stability of aerosol-generated NPs in liquid media provided insights into the behavior of supported NPs in different solvents and conditions,

shedding light on factors influencing stability and potential applications in various chemical environments. Considering the prevalence of gold and palladium NPs in heterogeneous catalysis, our findings re-emphasize the importance of stability and metal leaching in catalyst design and performance. The observed influences on NP adhesion, etching, and support material integrity underscore the importance of understanding the interplay between NPs, support materials, and solvents. The findings presented in this chapter and in Paper III offer essential guidance for future developments of high-performing supported aerosol-generated NPs for solvent-based applications.

5.3 Stability: NW supports

The NW structures were optimized to withstand the conditions during catalytic evaluations. As discussed above, the stability of the catalysts is important to correctly interpret the results when performing *ex situ* measurements. Therefore, the different nanowire designs were evaluated on their morphological stability and NP adhesion as they were immersed in methanol for 24 hours. The samples were characterized in SEM before and after exposure.

For the NPs on NW supports, it was not possible to perform a quantitative size- and density analysis or IL-SEM, as for the planar supports. Instead, a qualitative investigation of the stability was performed, where NW morphology and NP clustering and/or removal was investigated. A wide range of NW designs were tested, to find the optimized design to support the NPs during reaction. The criteria for the NW support design was: good NPs stability, i.e., no significant clustering or removal of the NPs; and similarly for the NWs, no severe NW clustering, and no morphological degradation. An excerpt of the results, where the samples had been immersed in methanol for 24 hours before removal, is presented in Figure 5.3.

It was found that, for very short wires, below $\sim$ 0.5 µm, all NPs were not collected by the NWs. Thus, although showing good NPs stability, such support designs are not suitable to use as catalyst supports. For very long wires and thin wires the immersion in methanol resulted in severe clustering, which is also not suitable for the catalytic evaluation. The designs which were concluded to be the most promising based on this study, was the designs shown in Figure 5.3 b) and c). These designs had complete collection of the NPs and had only a small amount of NW clustering, or none at all.

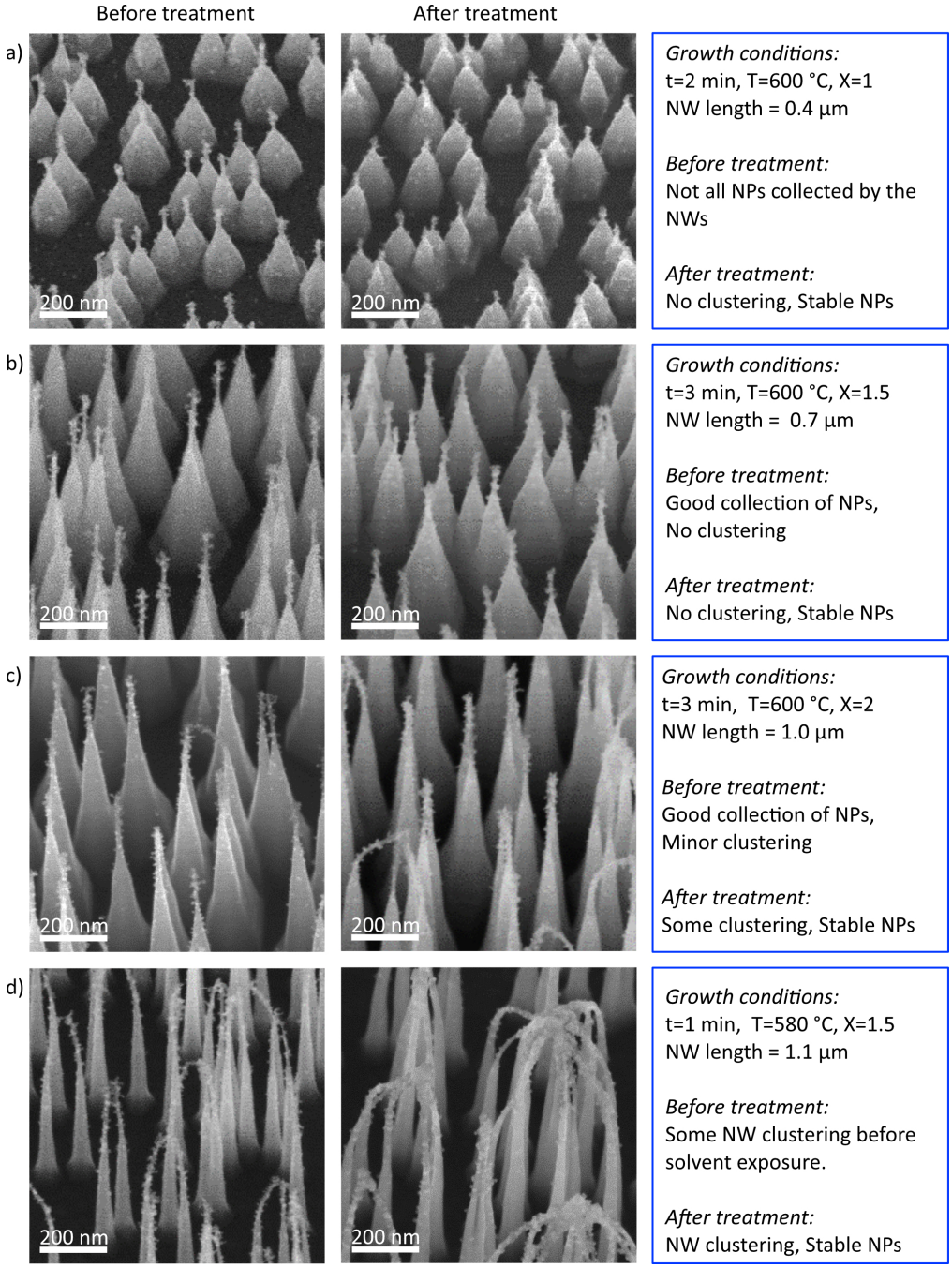

Figure 5.3: Pd NPs supported by different NW designs before and after treatment in methanol for 24 hours. The NWs were grown with different growth time, t, growth temperature, T, and precursor molar fraction, X (normalized to one for the lowest molar fraction). The V/III ratio was kept constant at 160.

After finding the optimal design based on the immersion into methanol, it was relevant to test the designs as catalysts in reaction. The reaction performed was hydrogenation of phenyl acetylene and more details on the general procedure is found in Chapter 6. The optimal design based on previous tests, was used as a catalyst. Although the catalyst displayed high catalytic activity, the post-reaction characterization in SEM showed that the nanowires were not stable during reaction. It appeared as if the tips had decomposed, see Figure 5.4 a). Because the tips were so narrow, the deposited NPs were positioned very densely on the tops. In particular, since the NWs behaved as antennas during the electrostatic deposition of the NPs, effectively collecting most of the NPs on the top parts of the NWs. Therefore, there was a high catalytic activity concentrated to the narrow tips, and any heat dissipated from the reaction might have contributed to the decomposition of the tips. This effect highlight the width of aspects that need to be considered when designing the nanostructures to be used as catalyst supports.

In order to remove the weakness of the structures, which in this case were the

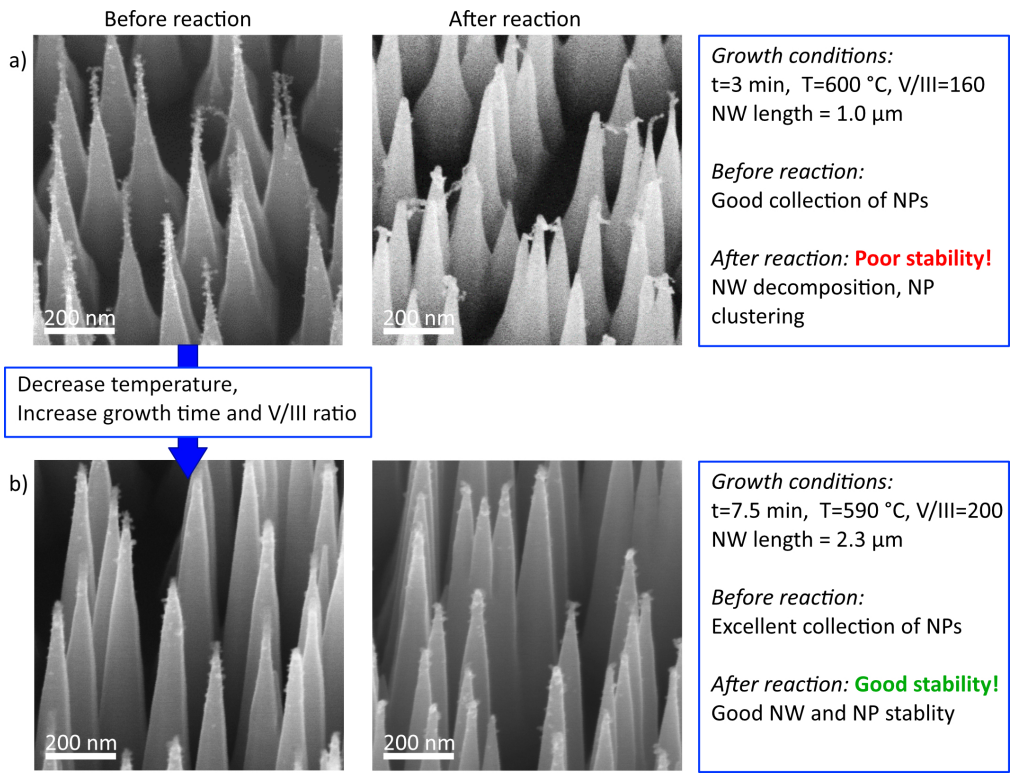

Figure 5.4: The optimized design from the immersion test, was used as catalyst for hydrogenation of phenyl acetylene.

narrow tips, the NWs were further developed. The V/III ratio was increased to increase the thickness, however, the resulting wires were too short. The temperature was decreased, which made the nanowire narrower but still too short. The growth time was increased, resulting in tall nanowires which were thick all the way to the tips, see Figure 5.4 b). This design was tested in reaction and showed good activity and stability, and this is the nanowire design used in the catalytic evaluation presented in Chapter 6.

5.3.1 Increased nanoparticle adhesion by RTP

As for the NPs on planar supports, the NP-NW system benefited in terms of enhanced stability by thermal processing. After deposition of the Pd NPs, the samples were annealed at 300 °C for 60 minutes in nitrogen gas. The effect of the annealing on the stability was tested by measuring the leaching during reaction. For this test, samples with two different NW support designs were included both with and without the final annealing step. After 10 hours of reaction, an aliquot of solution was removed from the reaction mixture and placed in a separate vial, and the catalytic conversion was measured. After a total of 24 hours, the catalytic conversion was measured again, both of the reaction mixture and of the removed aliquot. Leaching was determined by comparing the catalytic conversion of the aliquot after 24 hours with that of the reaction mixture measured at 10 hours. If the conversion in the aliquot was higher,

Table 5.1: Test of two different NW support designs, short and long, as well as the effect of rapid thermal processing (RTP) on leaching.

Sample info			Conversion of starting material (%)*			
			Catalytic reaction		Aliquot taken at t=10 h**	
Sample No.	NW type	RTP (Y/N)	10 h	24 h	24 h	Leaching (Y/N)
A1	Short	Y	4.4	30.7	4.1	N
A2	Short	N	22.7	86.7	29.2	Y
A3	Short	Y	5.2	53.8	5.3	N
B1	Short	N	0.9	6.5	4.8	Y
B2	Long	Y	15.9	64.2	15.6	N
B3	Long	N	8.2	52.2	35.4	Y
C1	Long	N	21.0	74.5	29.1	Y

* All samples were analyzed using GC-FID (Bruker) against naphthalene as an internal standard.

** A sample was taken and transferred to a new vial under a hydrogen atmosphere. It was analyzed at 24 h point using GC-FID against naphthalene as an internal standard. Conversion of >0.5 % compared to the 10 h mark indicates release of catalytically active species from the catalyst.

it showed that the conversion had continued even after removing it from the catalyst, indicating that the reaction was catalyzed by leached atoms or NPs.

The results, presented in Table 5.1, show that there was significant leaching only for the samples that were not annealed, regardless of the NW type. It was therefore possible to conclude that the post-processing step was important for the stability of the catalyst. However, this test was a crude measure of the leaching and could not detect very small amount of leaching. In order to confirm heterogeneity of a catalytic reaction, further testing is usually performed as part of the catalytic evaluation. This was also done for our catalyst, and is discussed in Chapter 6.

Chapter 6

Catalytic evaluation of solid-state nanostructures

Catalysts are vital components in a wide range of industrial processes [119]. Furthermore, many of these chemical processes include at least one hydrogenation step [120]. Semi-hydrogenation is an important group of reactions for the synthesis of fine chemicals, including pharmaceuticals and vitamins [121]. In particular, semi-hydrogenation of phenyl acetylene, which was the benchmark reaction chosen to evaluate the catalysts developed in this work, is an indispensable process in the polymer industry [122]. Improving the catalyst to increase the conversion efficiencies for these reactions would result in substantial savings both in cost and energy.

In the chapters leading up to this one, the different aspects of the development of the catalysts are treated. Here, they are combined in a modular fabrication approach and the catalytic performance is evaluated. The results in this chapter are based on Paper IV.

6.1 Nanocatalysis

A catalyst changes the rate of a reaction by offering an alternative pathway for the reaction. In heterogeneous catalysis, the alternative pathway typically includes adsorption of the reactants onto the catalyst surface, effectively reducing the strength of the internal bonds and, thereby, decreasing the activation energy of the reaction.

The term nanocatalysis refers to catalysis by structures that are nano-sized (in at least two directions), leading to effects such as high surface-to-volume ratios and high energy surface sites, which are beneficial for the catalytic performance. In an industrial reactor, the catalyst often consists of NPs embedded in a porous oxide, and is exposed to high pressures and temperatures. Such catalysts can achieve very high activity [123], however, fundamental evaluation of an industrial catalyst is difficult. The NPs are typically distributed onto an irregularly shaped support, thus, the catalytic response will be an average response from many different types of active sites with various accessibility from the reactants.

Simplified model systems, such as single crystals, have been used to study the reaction on specific surface sites [124]. From the studies of single crystals it has been possible to understand the relative reactivity of the surface, as well as how the molecules are adsorbed onto the surface. The field of surface science has evolved to enable *in situ* studies of catalytic reactions with the more complex structures of curved surfaces, nanocrystals, and NPs [125–128]. Such studies provide valuable information about the sites at low-index planes and facets, which are typically more catalytically active. However, in order to perform these detailed surface studies, the conditions need to be very far from those of industrial reactors in terms of pressure and temperature, and the reactions studied are, to a large extent, relatively simple gas-phase reactions. To study the reactions involving more complex organic synthesis, the approach need to be more deductive since the evaluation is performed *ex situ*. For this approach it is beneficial to have a model catalyst where the different parameters involved, such as size, chemical composition, and crystallinity can be controlled individually.

A challenge in catalyst development is to achieve high chemoselectivity for the specific chemical reaction. Chemoselectivity refers to the ability to selectively react with one functional group in the presence of multiple functional groups in a molecule and it plays an important role in reducing waste and energy [129]. In the case of semi-hydrogenation, the challenge often lies in avoiding overhydrogenation. For the semi-hydrogenation of acetylenically unsaturated compounds a functional catalysts was developed by Lindlar and named thereafter [130]. The Lindlar catalyst is based on Pd NPs that are partially deactivated by lead, resulting in increased chemoselectivity [131]. However, since there are clear policies to remove all use of lead in production, there is much research focusing on finding alternatives that are more environmentally friendly [132].

As is shown in the catalytic evaluation below, the Pd NPs generated by the spark discharge generator, show a remarkable selectivity in favor of the partially reduced product. Since the method of spark ablation is free of any chemical waste product, these particles are interesting candidates for a green replacement

to the Lindlar catalyst. The combination with the NW supports which provide high control over the morphology over large surface areas, equips us with a highly interesting model system for systematic studies of catalyzed organic synthesis.

6.2 Modular fabrication of the catalyst

The purpose of this work was to explore a new modular approach to developing catalyst that enables isolated tuning of the parameters that have an effect on the catalytic performance. As a proof-of-concept, a comparison was made between the catalytic response from Pd NPs deposited on a planar support to NPs elevated from the surface by tapered NWs.

In this section, the fabrication of the catalysts is summarized, and more details on the methodologies used for NP generation, NW growth, and stability evaluation is found in the previous chapters. The catalyst fabrication included three parts, preparation of the supports (Figure 6.1 a), NP generation and deposition (Figure 6.1 b), and post-processing (Figure 6.1 c).

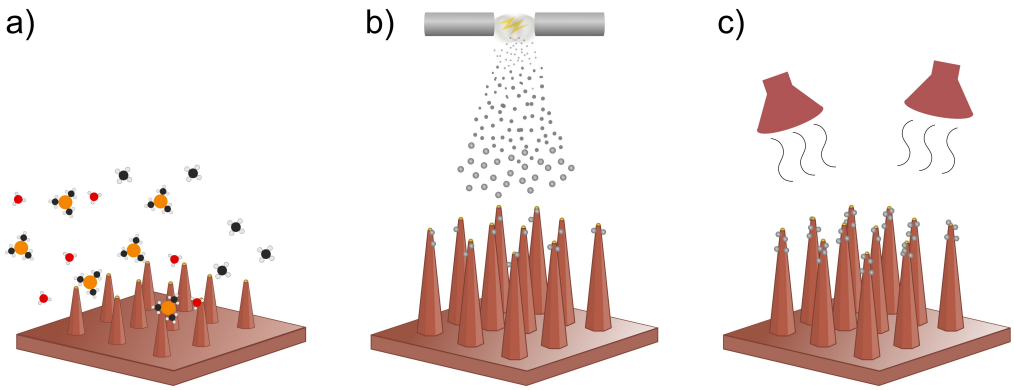

Figure 6.1: Modular fabrication of catalysts, including three main components: a) design, development and preparation of the nanostructured support; b) generation and deposition of catalytic NPs; and c) post-processing for increased stability during reaction.

Preparing the supports

The supports were based on GaP (111)B wafers, cut into 8 mm x 8 mm pieces using an automatic dicing saw (Disco DAD 3320). Gold seed NPs with a diameter of 10 nm were deposited by E/C with a concentration of 40 μm^{-2}. The NWs were grown at 590 °C for 7.5 minutes, using TMGa and PH_3 precursors. The planar supports were produced according to the same procedure as for the

NWs, with the one difference that no TMGa was introduced during the growth step, so that no NWs were grown. In all other aspects, the NW and planar supports were prepared in the same way.

Generating the catalytic nanoparticles

After the NW (or planar) growth, the samples were transferred to the ESP connected to the SDG. In the SDG, the catalytic NPs were generated, sintered into a spherical shape, size-selected for a narrow size distribution, and deposited electrostatically onto the support. For the results presented here, Pd NPs were used, size-selected to 10 nm and deposited with a concentration of 1000 μm^{-2}. For the NW supports, the NWs acted as antennas and attracted the NPs to be positioned mostly on the top part of the NWs during deposition. The strength of this effect could in principle be controlled by the voltage applied to the ESP.

Post-processing

Finally, the sample was placed in a Rapid Thermal Processing (RTP) system (RTP-1200-100 from UniTemp GmbH) for annealing of the deposited particles at 300 °C for 60 minutes. This was done to increase the adhesion of the NPs to the support and to enhance the stability of the catalyst during reaction, as was discussed in Chapter 5.

6.3 Catalytic evaluation

In this section, the work on evaluating the catalytic performance of the catalysts is presented.

6.3.1 Metrics for evaluating the catalytic activity

When evaluating the catalytic performance, there are a few important metrics that need to be defined. The conversion, $C(t)$, of a species with initial concentration, A_0, and concentration, A_t, after time, t:

$$C(t) = \frac{A_0 - A_t}{A_0} \tag{6.1}$$

The selectivity, S, in favor of product A_1, between two possible products, A_1, and A_2, at time, t, is given by:

$$S = \frac{A_{1,t}}{\sum_{n=1,2} A_{n,t}} \tag{6.2}$$

When studying the catalytic activity, it is interesting to consider the amount of converted product in relation to the catalytically active material, which is given by the *Turn-Over-Number* (TON):

$$TON = \frac{\text{converted product (mol)}}{\text{catalyst (mol)}} \tag{6.3}$$

There are some variations in the literature on how the amount of catalyst used in the TON is determined. In some cases, only the surface atoms are given, or, in some cases, only the active sites. This results in higher TON as compared to using the total amount of catalytic material, as is used here. This is something that needs to be considered when comparing different results from literature.

The rate of the reaction, or the *Turn-Over-Frequency* (TOF), can simply be expressed as the TON divided by the time of reaction:

$$TOF = \frac{TON\ (\text{mol} \cdot \text{mol}^{-1})}{\text{time of reaction}\ (s)} \tag{6.4}$$

Also in the case of TOF, there are variations in the definition, mostly in terms of time range, where the momentary TOF in the beginning of the reaction can yield different results than the total average rate, which was used in this work, if the reaction rate is not constant.

6.3.2 Experimental set-up

The catalytic properties of the NW-system were evaluated in partial hydrogenation of phenylacetylene. A high-vacuum/hydrogen line, shown in Figure 6.2 a) and schematically in b), was used to provide a hydrogen to the reaction mixture with a constant pressure. This was necessary, since the reaction rate was found to be very sensitive to the hydrogen pressure. In an initial set-up, regular balloons filled with hydrogen were used to provide hydrogen to the reaction. In this case, the pressure dropped as the hydrogen was consumed, resulting in a

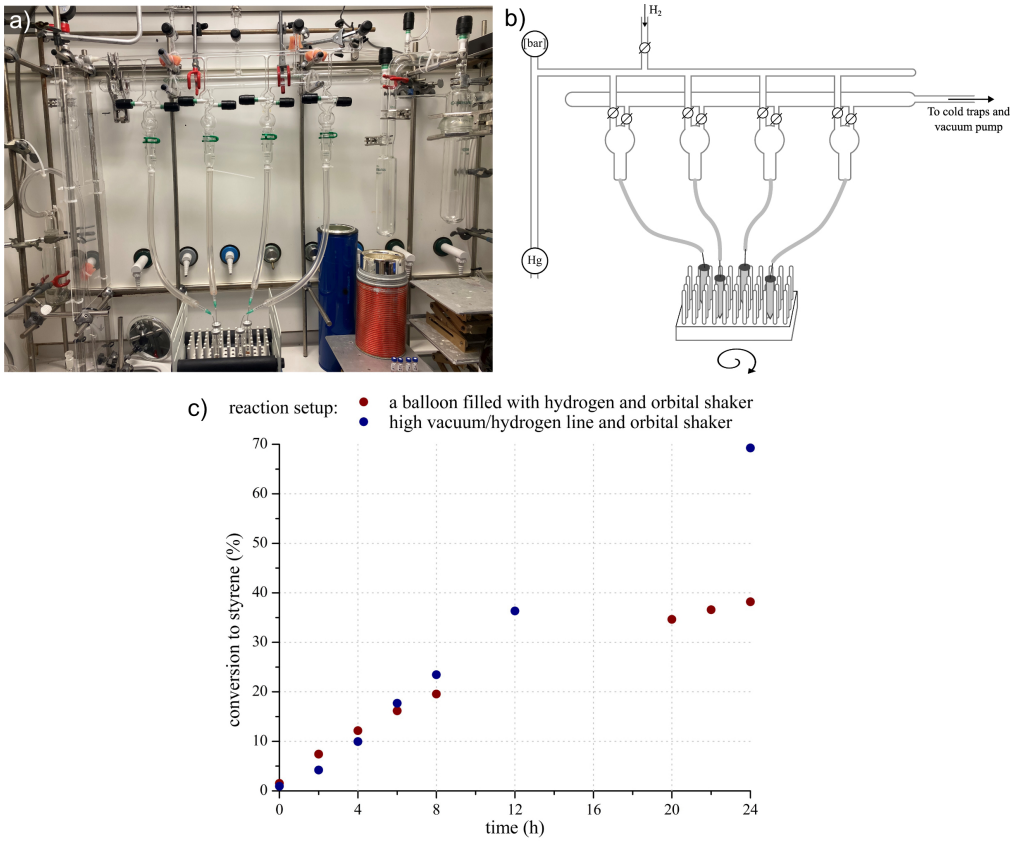

Figure 6.2: The set-up for the catalytic evaluation consisted of a high vacuum/hydrogen line and orbital shaker shown in a) and schematically in b). This set-up feeds the reaction mixtures with a constant hydrogen pressure, resulting in a constant conversion rate, as compared to the decreased rate with time when the hydrogen was provided by hydrogen-filled balloons. (c).

decrease in reaction rate, as can be seen in Figure 6.2 c). Oven-dried microwave vials were used for the reaction mixture and were placed in an orbital shaker. The orbital shaker provided good mass-transport to the catalyst and was used as an alternative to a traditional stirring magnet, which could cause mechanical damage to the catalyst.

The kinetics of the catalyzed reactions were evaluated using gas chromatography (GC), performed using a Bruker 430-GC. GC is a common tool for chemical analysis and gives a quantitative measure with a low limit of detection of the compounds present in the reaction mixture. In some cases, where a more qualitative measure was relevant, H^1 nuclear magnetic resonance (NMR) was employed, using a Bruker AVANCE II 400 MHz. This was used specifically when evaluating the three-phase test of heterogenicity.

6.3.3 Results

The first part of the catalytic evaluation was a solvent screening to identify the optimal solvent for this system. Seven different solvents, both polar and apolar, were included in the optimization study, and the resulting conversions and selectivity achieved by the NW-catalyst are found in Table 6.1. Acetone, which is a cheap and environmentally benign solvent, was the solvent used in the reaction with the highest reaction rate along with excellent selectivity ($> 98\,\%$ of the partially hydrogenated product). It was thus chosen as the solvent for the kinetic studies of the different type of catalysts.

Table 6.1: Solvent optimization conducted with a PdNP-GaPNW catalyst.[a]

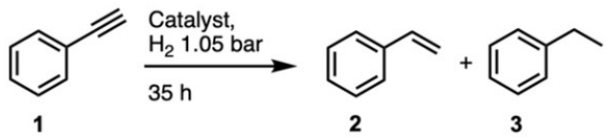

Entry	Solvent	Conversion (mmol)	Selectivity (2/3)
1.	Acetone	0.073	98.3/1.7
2.	Methanol	0.031	98.2/1.8
3.	1-Butanol	0.031	98.2/1.8
4.	Dioxane	0.033	97.3/2.7
5.	Dichloromethane	0.0017	Not determined
6.	Hexane	-[b]	-
7.	Toluene	-[b]	-

a) *General procedure:* The catalyst was activated by exposure to H_2 (1.05 bar) for 15 min. Phenylacetylene (0.01 µL, 0.09 mmol) was then introduced along with the indicated solvent (2.0 mL). Reaction progress was monitored by GC using bicyclohexyl as an internal standard. b) No conversion observed.

The next step was to evaluate the performance of the NW catalyst as compared to the planar catalyst and the Lindlar catalyst. The Lindlar catalyst was included as a reference since it is the benchmark catalyst for hydrogenation of alkynes. The resulting TOFs, displayed in Figure 6.3, show that the NW-catalysts had a 15-fold increase in activity as compared to the planar-catalysts, and a 10-fold increase in activity compared to the Lindlar catalyst. This is a remarkable difference achieved by elevating the NPs about 2 µm from the planar surface. In addition to being elevated from the surface, the NPs are also positioned on a curved surface, which means that the contact angle between the NPs and the support changes, which can give rise to more active centers for catalysis [133].

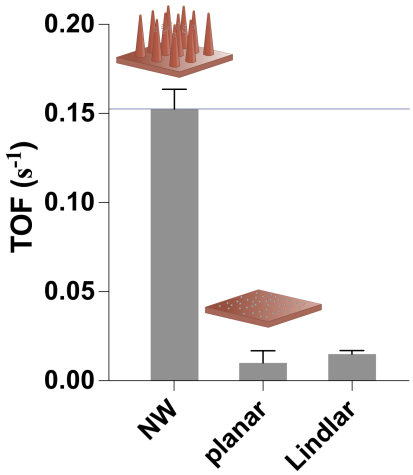

Figure 6.3: TOF for NW-catalysts, planar catalysts, and Lindlar catalyst in the reduction of phenylacetylene. TOF values were calculated from rate constants obtained from the linear regression of $\ln(C_t/C_0)$ and given as mean $\pm$ SEM (n = 4, two replicates in each).

Before and after used in reaction, the catalysts were characterized by SEM and (HR)TEM, in order to detect any morphological changes. It was found that the NPs remained on the NWs without any significant changes. The NW mor-

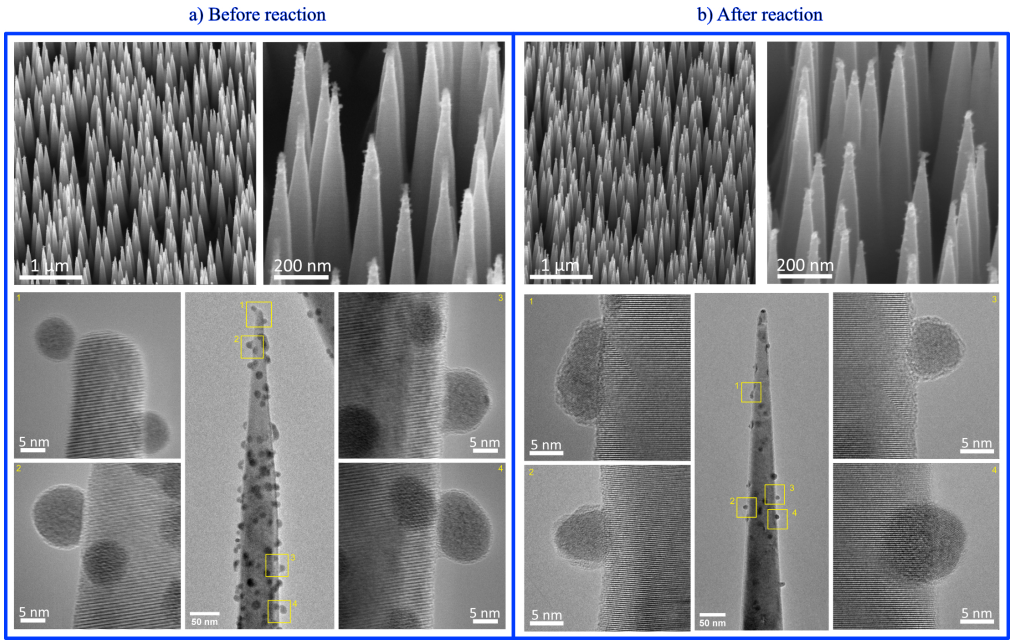

Figure 6.4: SEM and (HR)TEM a) before and b) after use for hydrogenation of phenylacetylene. SEM images show that the general morphology is stable during reaction. From HRTEM it is also clear that the NPs are mainly intact.

phology also remain the same as before reaction. However, HRTEM on the NP decorated NWs after reaction reveal that some of the NPs have merged with the NW (see Figure 6.4). This was observed only for NPs very close to the tips of the NWs, where the NWs are the thinnest and also most accessible to the reaction mixtures. It is possible that these NPs have caused some decomposition of the NWs and that this is the same effect that caused the more severe decomposition for the NW design with the thinner tips, shown in Figure 5.4.

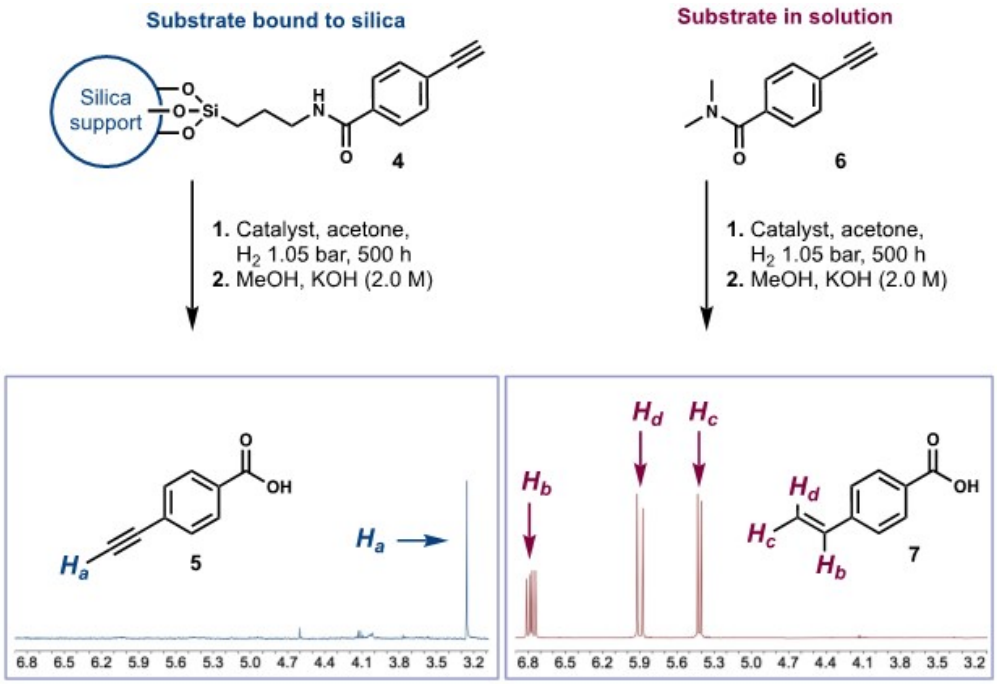

Figure 6.5: Three-phase test of heterogenicity. Only signals corresponding to non-reduced alkyne **4** are seen in the NMR spectrum after hydrolytic release (left). Efficient partial hydrogenation of alkyne 6 confirmed by signals corresponding to vinylene **7** after hydrolysis (right).

A three-phase test was conducted to evaluate the heterogenicity of the catalytic reaction [134, 135]. This test is important as it answers the fundamental question – is the reaction catalyzed by the solid catalyst (heterogeneous catalysis) or by leached atoms (homogeneous catalysis) For the three-phase test, the substrate, which here refers to the molecule which is the subject for the catalyzed reaction, is bound to a solid, in this case silica, support and separated from the solid catalyst by the solvent. Then the reaction is conducted according to the general procedure and after a certain time, 500 hours in this case, the reaction is stopped and the substrate is hydrolyzed, effectively removing the substrate from the solid support, so that it can be analyzed. The same is done for the corresponding

substrate in solution, as a reference.

The analysis was performed with NMR and the resulting spectra from the solid-bound substrate and for the substrate in solution are found in Figure 6.5. The spectra reveal that there had been no hydrogenation of solid-bound spectra, while the substrate in solution had been completely consumed. From these results it is possible to conclude that the catalyzed reaction is completely heterogeneous, and no leaching of the catalyst occurs.

In summary, in this chapter I have shown that the NW-supported Pd NPs are highly catalytically active, with a conversion rate 15 times that of the planar-supported catalyst. The NW-supported catalyst are also highly selective, exceeding even what has been reported for the Lindlar catalyst. Finally, characterization by electron microscopy and three-phase heterogenicity test show that the catalyst is highly stable in reaction.

Chapter 7

Conclusions and Outlook

The goal of this thesis was to develop a new approach to catalyst design by integrating nanotechnology with organic synthesis. As I complete the end of my doctoral studies it is appropriate to evaluate this approach and its future.

In this doctoral thesis, I am presenting a novel approach to the design and development of solid-state nanostructures for catalysis. This method offers a comprehensive framework for isolating and understanding the various parameters influencing the catalytic response of the nanostructures, and it encompasses three main components: the generation of catalytic nanoparticles, the fabrication of the nanostructure support, and post-processing techniques designed to enhance stability.

Starting with the production of nanoparticles. I have used aerosol methods, particularly the spark discharge generator, based on spark ablation, as a versatile tool for tailoring the nanoparticle properties. The choice of aerosol-based methods for generating nanoparticles can easily be motivated as solvent-free alternative to chemical synthesis methods. However, it is perhaps more relevant to benchmark spark ablation to other gas-phase methods, such as magnetosputtering, which can also provide high purity nanoparticles with good compositional control. What I have experienced during my research, is that the spark discharge generator is a low-maintenance, stable, and easily adaptable tool which is compatible with many aerosol instruments for analysis of various kinds. From my measurements I have also observed that the quality of the generated nanoparticles is pristine in terms of crystallinity, mixing, purity, reproducibility.

The property I chose to focus on was the chemical composition of Pd-Cu bimet-

allic nanoparticles. Through systematic investigations, I have demonstrated the remarkable level of control achievable by simply altering the electrode materials, switching between pure and alloyed electrodes. This versatility has paved the way for precise tuning of nanoparticle characteristics. From the time-resolved XRF measurements it was observed that, in general, the compositional stability was very high. However, while studying the generation of bimetallic nanoparticles by spark ablation, it has also became clear that the processes that occur during the moment of the spark and the brief moment afterwards, is highly complex and encompasses aspects related to a wide range of fields, including electronics, plasma physics, fluid dynamics, and – of course – aerosol physics. To truly understand these processes, a combination of modelling, simulations, and systematic experimental studies will be necessary.

For the development of the support-structures, where close-packed tapered GaP NWs were utilized, the key aspect was to develop structures that were mechanically and chemically stable, both in solution and during reaction. This, seemingly simple task ended up being one of the largest obstacles to achieving stable catalysts for evaluation. One of the most surprising aspects during the development of the nanowire supports structures was the impact of the catalytic activity. A catalyst that was perfectly stable in the reaction environment was found to severely decompose once the reactants were added and catalytic conversion occurred. The final design was developed to have a thick top part, which contributed not only to increased mechanical stability, but also to spread out the NPs a bit more over the surface, and this design was shown to be stable in reaction.

For the catalytic evaluation I was pleased to report such promising results for the NW-supported Pd NP catalyst. The effect from elevating the Pd NPs from the surface resulted in a TOF which was an order of magnitude higher than for the planar-support, as well as for the Lindlar catalyst, which is the benchmark catalyst for semihydrogenation of alkynes. The complete absence of leaching as measured by the three phase test of heterogenicity is also promising for the potential of recyclability of the catalyst.

Looking ahead, this research opens exciting questions for further exploration and development. I anticipate that the insights gained from our work will serve as a foundation for refining and expanding the capabilities of this novel approach. The ability to isolate and manipulate key parameters responsible for the catalytic performance holds large potential in the field of catalysis. Future research can focus on refining and extending the control over the different components of the modular catalyst.

The effect of the bimetallic nanoparticle composition and crystal structure on their catalytic performance should be evaluated. The system current set-up allows for separation of the compositional tuning from any other changes of the catalyst, to truly isolate its effect. Furthermore, the bimetallic system can easily be extended to multimetallic, by using two pre-alloyed electrodes of different materials. This way, high entropy alloys could be achieved which might have very interesting catalytic properties [136].

The Pd-seeded nanowires and nanotrees have yet to be tested as catalysts. The first step would be to replace the Au-seeded nanowires by the Pd-seeded nanowires, to see if the the presence of Au had any effect on the catalytic performance. Furthermore, the nanotrees should be tested on their own, letting the Pd-seed particles act as the active catalysts. In this case, careful evaluation of the seed particles composition and crystal structure is necessary, as both Ga and Pd might be incorporated in the particles, resulting in interesting phases.

Further investigations on the catalytic applications of the nanoparticle-decorated nanowires should be performed, expanding their applications to other reactions, both hydrogenation reactions, and C–C coupling reactions. For these reactions it will also be relevant to compare the activity for our catalysts with the ones used in industry. In this work we have compared the developed catalysts to the benchmark catalyst for this reaction, and concluded that it performs very well. However, we do not yet know how he catalysts would compare in the high pressures and temperatures typically associated with industrial processes. Do we find that they are efficient enough to use at ambient pressure and temperature? Such a catalyst would have the potential to save a lot in energy and cost in the processes.

References

[1] G. Rupprechter. *Surface Science Approach to Heterogeneous Catalysis*, chapter 39, pages 459–528. John Wiley Sons, Ltd, 2016.

[2] K.D. Vogiatzis, M.V. Polynski, J.K. Kirkland, J. Townsend, A. Hashemi, C. Liu, and E.A. Pidko. Computational Approach to Molecular Catalysis by 3d Transition Metals: Challenges and Opportunities. *Chemical Reviews*, 119(4):2453–2523, 2019.

[3] J. W. Erisman, M.A. Sutton, J. Galloway, Z Klimont, and W. Winiwarter. How a century of ammonia synthesis changed the world. *Nature Geoscience*, 1(October 1908):636–639, 2008.

[4] I. Chorkendorff. *Concepts of Modern Catalysis and Kinetics.*, volume 3rd ed. Wiley-VCH, 2017.

[5] K.W. Kolasinski. *Surface science. Foundations of catalysis and nanoscience.* Wiley, 2012.

[6] L. Österlund. *Pressure Gaps in Heterogeneous Catalysis*, chapter 13, pages 225–251. John Wiley Sons, Ltd, 2021.

[7] D.J. Cole-Hamilton. Homogeneous catalysis–new approaches to catalyst separation, recovery, and recycling. *Science*, 299(5613):1702–1706, 2003.

[8] P. Serp and K. Philippot. *Nanomaterials in catalysis.* Wiley-VCH, 2013.

[9] D. Astruc. *Nanoparticles and Catalysis.* Wiley-VCH, 2008.

[10] T. Ishida and M. Haruta. Gold catalysts: Towards sustainable chemistry. *Angewandte Chemie International Edition*, 46(38):7154–7156, 2007.

[11] V. Polshettiwar and T. Asefa. *Introduction to Nanocatalysis*, chapter 1, pages 1–9. John Wiley Sons, Ltd, 2013.

[12] M. Sankar, N. Dimitratos, P.J. Miedziak, P.P. Wells, C.J. Kiely, and G.J. Hutchings. Designing bimetallic catalysts for a green and sustainable future. *Chemical Society Reviews*, 41(24):8099–8139, 2012.

[13] Z. Wei, J. Sun, Y. Li, A.K. Datye, and Y. Wang. Bimetallic catalysts for hydrogen generation. *Chemical Society Reviews*, 41(24):7994–8008, 2012.

[14] S. Dang, H. Yang, P. Gao, H. Wang, X. Li, W. Wei, and Y. Sun. A review of research progress on heterogeneous catalysts for methanol synthesis from carbon dioxide hydrogenation. *Catalysis Today*, 330:61–75, 2019.

[15] M. Ullmann, S.K. Friedlander, and A. Schmidt-ott. Nanoparticle formation by laser ablation. *Journal of Nanoparticle Research*, 4:499–509, 2002.

[16] Q. Fu, D. Kokalj, D. Stangier, F.E. Kruis, and W. Tillmann. Aerosol synthesis of titanium nitride nanoparticles by direct current arc discharge method. *Advanced Powder Technology*, 31(9):4119–4128, 2020.

[17] M.H. Magnusson, K. Deppert, J.-O. Malm, J.-O. Bovin, and L. Samuelson. Gold nanoparticles: Production, reshaping, and thermal charging. *Journal of Nanoparticle Research*, 1:243–251, 1999.

[18] N.S. Tabrizi, M. Ullmann, V.A. Vons, U. Lafont, and A. Schmidt-Ott. Generation of nanoparticles by spark discharge. *Journal of Nanoparticle Research*, 11(2):315–332, 2009.

[19] B.O. Meuller, A.M. Jansson, L.I.M. Johansson, N. Tureson, D.L.J. Engberg, M.E. Messing, K. Deppert, and S.M. Norlén. Review of Spark Discharge Generators for Production of Nanoparticle Aerosols. *Aerosol Science and Technology*, 46(11):1256–1270, 2012.

[20] A. Schmidt-Ott. *Spark Ablation: Building Blocks for Nanotechnology.* Jenny Stanford Publishing Pte. Ltd., 2020.

[21] R. T. Hallberg, L. Ludvigsson, C. Preger, B. O. Meuller, K. A. Dick, and M. E. Messing. Hydrogen-assisted spark discharge generated metal nanoparticles to prevent oxide formation. *Aerosol Science and Technology*, 52(3):347–358, 2018.

[22] K.F. Jensen, D.I. Fotiadis, and T.J. Mountziaris. Detailed models of the MOVPE process. *Journal of Crystal Growth*, 107(1-4):1–11, 1991.

[23] J. Wu, B.M. Borg, D. Jacobsson, K.A. Dick, and L.-E. Wernersson. Control of composition and morphology in InGaAs nanowires grown by metalorganic vapor phase epitaxy. *Journal of Crystal Growth*, 383:158–165, 2013.

[24] S.Y. Karpov. Advances in the modeling of MOVPE processes. *Journal of Crystal Growth*, 248(SUPPL.):1–7, 2003.

[25] J. Wallentin, N. Anttu, D. Asoli, M. Huffman, I. Åberg, B. Witzigmann, H.Q. Xu, L. Samuelson, K. Deppert, and M.T. Borgström. InP Nanowire Array Solar Cells Achieving 13.8Exceeding the Ray Optics Limit. *Science*, 339(6123):1057–1060, 2013.

[26] A. Pandey, J. Min, M. Reddeppa, Y. Malhotra, Y. Xiao, Y. Wu, K. Sun, and Z. Mi. An Ultrahigh Efficiency Excitonic Micro-LED. *Nano Letters*, 23(5):1680–1687, 2023.

[27] N.S. Ramgir, Y. Yang, and M. Zacharias. Nanowire-based sensors. *Small*, 6(16):1705–1722, 2010.

[28] D. Verardo, L. Liljedahl, C. Richter, B. Agnarsson, U. Axelsson, C.N. Prinz, F. Höök, C.A.K. Borrebaeck, and H. Linke. Fluorescence signal enhancement in antibody microarrays using lightguiding nanowires. *Nanomaterials*, 11(1):1–11, 2021.

[29] M. Garg, A. Martin-Jimenez, Y. Luo, and K. Kern. Ultrafast Photon-Induced Tunneling Microscopy. *ACS Nano*, 15(11):18071–18084, 2021.

[30] A.E. Vladár and V.-D. Hodoroaba. Chapter 2.1.1 - characterization of nanoparticles by scanning electron microscopy. In V.-D. Hodoroaba, E.S. Unger, W, and A.G. Shard, editors, *Characterization of Nanoparticles*, Micro and Nano Technologies, pages 7–27. Elsevier, 2020.

[31] D.B. Williams and C.B. Carter. *Transmission Electron Microscopy: A Textbook for Material Science*. Number Mi. Springer Science+Business Media, New York, 2nd editio edition, 2009.

[32] E. Ruska. The development of the electron microscope and of electron microscopy (nobel lecture). *Angewandte Chemie International Edition in English*, 26(7):595–605, 1987.

[33] W. Zhou, R. Apkarian, Z.L. Wang, and D. Joy. *Fundamentals of Scanning Electron Microscopy (SEM)*, pages 1–40. Springer New York, New York, NY, 2007.

[34] G. Thomas. Modern electron microscopy for materials characterization. *Journal of Electron Microscopy Technique*, 3(1):95–108, 1986.

[35] R. Gauvin. Review of transmission electron microscopy for the characterization of materials. *Materials Characterization and Optical Probe Techniques: A Critical Review*, 10291(July 1997):102910C, 1997.

[36] E. J. Milton. Review article principles of field spectroscopy. *International Journal of Remote Sensing*, 8(12):1807–1827, 1987.

[37] P.J. Potts and P.C. Webb. X-ray Fluorescence Spectrometry. *Journal of Geochemical Exploration*, 44:251–296, 1992.

[38] F.A. Stevie and C.L. Donley. Introduction to x-ray photoelectron spectroscopy. *Journal of Vacuum Science Technology A: Vacuum, Surfaces, and Films*, 38(6), 2020.

[39] N. Krasteva, I. Besnard, B. Guse, R.E. Bauer, K. Müllen, A. Yasuda, and T. Vossmeyer. Self-Assembled Gold Nanoparticle/Dendrimer Composite Films for Vapor Sensing Applications. *Nano Letters*, 2(5):551–555, 2002.

[40] A. Bellacicca, T. Santaniello, and P. Milani. Embedding electronics in 3D printed structures by combining fused filament fabrication and supersonic cluster beam deposition. *Additive Manufacturing*, 24(September):60–66, 2018.

[41] J.H. Byeon and J.T. Roberts. Aerosol-based fabrication of biocompatible organicinorganic nanocomposites. *ACS Applied Materials and Interfaces*, 4(5):2693–2698, 2012.

[42] D. Astruc. Introduction: Nanoparticles in Catalysis. *Chemical Reviews*, 120(2):461–463, 2020.

[43] J. Feng, G. Biskos, and A. Schmidt-Ott. Toward industrial scale synthesis of ultrapure singlet nanoparticles with controllable sizes in a continuous gas-phase process. *Scientific Reports*, 5(October):1–9, 2015.

[44] E. Pratsinis. Flame Aerosol Synthesis of Ceramic Powders. 24(97):197–219, 1998.

[45] R. Strobel, A. Baiker, and S.E. Pratsinis. Aerosol flame synthesis of catalysts. *Advanced Powder Technology*, 17(5):457–480, 2006.

[46] A. Jaworek and A.T. Sobczyk. Electrospraying route to nanotechnology: An overview. *Journal of Electrostatics*, 66(3-4):197–219, 2008.

[47] D. Llamosa, M. Ruano, L. Martínez, A. Mayoral, E. Roman, and Y. Huttel. The ultimate step towards a tailored engineering of core@shell and core@shell@shell nanoparticles. *Nanoscale*, 6(22), 2014.

[48] Y. Huttel and L. Martínez. Gas-phase synthesis of nanoparticles : present status and perspectives. 8(3):947–954, 2018.

[49] Y. Singh, J.R.N. Javier, S.H. Ehrman, M.H. Magnusson, and K. Deppert. Approaches to increasing yield in evaporation/condensation nanoparticle generation. *Journal of Aerosol Science*, 33(9):1309–1325, 2002.

[50] A. Schmidt-Ott. New approaches to in situ characterization of ultrafine agglomerates. *Journal of Aerosol Science*, 19(5), 1988.

[51] J.-P. Borra. Nucleation and aerosol processing in atmospheric pressure electrical discharges : powders production , coatings. *Journal of Physics D: Applied Physics*, 39:R19–R54, 2006.

[52] J.H. Byeon, J.H. Park, and J. Hwang. Spark generation of monometallic and bimetallic aerosol nanoparticles. *Journal of Aerosol Science*, 39(10):888–896, 2008.

[53] N.S. Tabrizi, Q. Xu, N.M. Van Der Pers, U. Lafont, and A. Schmidt-Ott. Synthesis of mixed metallic nanoparticles by spark discharge. *Journal of Nanoparticle Research*, 11(5):1209–1218, 2009.

[54] N.S. Tabrizi, Q. Xu, N. M. Van Der Pers, and Andreas Schmidt-Ott. Generation of mixed metallic nanoparticles from immiscible metals by spark discharge. *J Nanopart Res*, pages 247–259, 2010.

[55] A. Muntean, M. Wagner, J. Meyer, and M. Seipenbusch. Generation of copper, nickel, and CuNi alloy nanoparticles by spark discharge. *Journal of Nanoparticle Research*, 18(8), 2016.

[56] J. Feng, N. Ramlawi, G. Biskos, and A. Schmidt-Ott. Internally mixed nanoparticles from oscillatory spark ablation between electrodes of different materials. *Aerosol Science and Technology*, 52(5):505–514, 2018.

[57] F. Llewellyn Jones. Electrode erosion by spark discharges. *British Journal of Applied Physics*, 1(3):60–65, 1950.

[58] L. Ludvigsson, B.O. Meuller, and M.E. Messing. Investigations of initial particle stages during spark discharge. *Journal of Physics D: Applied Physics*, 48(31):314012, 2015.

[59] C.R. Svensson, L. Ludvigsson, B.O. Meuller, M.L. Eggersdorfer, K. Deppert, M. Bohgard, J.H. Pagels, M.E. Messing, and J. Rissler. Characteristics of airborne gold aggregates generated by spark discharge and high temperature evaporation furnace: Mass-mobility relationship and surface area. *Journal of Aerosol Science*, 87:38–52, 2015.

[60] A. Wiedensohler. An approximation of the bipolar charge distribution for particles in the submicron size range. *Journal of Aerosol Science*, 19(3):387–389, 1988.

[61] E.O. Knutson and K.T. Whitby. Aerosol classification by electric mobility: apparatus, theory, and applications. *Journal of Aerosol Science*, 6(6):443–451, 1975.

[62] W.C. Hinds. *Aerosol Technology: Properties, Behavior, and Measurement of Airborne Particles, 2nd Edition*. Wiley-Interscience, 1999.

[63] K. Deppert, F. Schmidt, T. Krinke, J. Dixkens, and H. Fissan. Electrostatic precipitator for homogeneous deposition of ultrafine particles to create quantum-dot structures. *Journal of Aerosol Science*, 27(SUPPL.1):2–3, 1996.

[64] C. Preger, N.C. Overgaard, M.E. Messing, and M.H. Magnusson. Predicting the deposition spot radius and the nanoparticle concentration distribution in an electrostatic precipitator. *Aerosol Science and Technology*, 54(6):718–728, 2020.

[65] B. Liu, S. Liu, V. Devaraj, J. Ai, Y. Han, and J. Feng. Metal 3D nanoprinting with coupled fi elds. (March):1–11, 2023.

[66] R. Mandal, A. Baranwal, A. Srivastava, and P. Chandra. Evolving trends in bio/chemical sensor fabrication incorporating bimetallic nanoparticles. *Biosensors and Bioelectronics*, 117(April):546–561, 2018.

[67] R. Rajeev, R. Datta, A. Varghese, Y.N. Sudhakar, and L. George. Recent advances in bimetallic based nanostructures: Synthesis and electrochemical sensing applications. *Microchemical Journal*, 163(December 2020):105910, 2021.

[68] Y.H. Jo, I. Jung, N.R. Kim, and H.M. Lee. Synthesis and characterization of highly conductive Sn-Ag bimetallic nanoparticles for printed electronics. *Journal of Nanoparticle Research*, 14(4), 2012.

[69] H.W. Tan, J. An, C.K. Chua, and T. Tran. Metallic Nanoparticle Inks for 3D Printing of Electronics. *Advanced Electronic Materials*, 5(5), 2019.

[70] S. Xiong, W. Qi, B.n Huang, and M. Wang. Size-, shape- and composition-dependent alloying ability of bimetallic nanoparticles. *ChemPhysChem*, 12(7):1317–1324, 2011.

[71] A. Kohut, Lajos P. Villy, A. Kéri, Á. Bélteki, D. Megyeri, B. Hopp, G. Galbács, and Z. Geretovszky. Full range tuning of the composition of Au/Ag binary nanoparticles by spark discharge generation. *Scientific Reports*, 11(1):1–10, 2021.

[72] R.R. Lapierre, M. Robson, K.M. Azizur-Rahman, and P. Kuyanov. A review of III – V nanowire infrared photodetectors and sensors. *Journal of Physics D: Applied Physics TOPICAL*, 50:123001, 2017.

[73] H. Riel, L.-E. Wernersson, M. Hong, and J.A. Alamo. III – V compound semiconductor transistors — from planar to nanowire structures. *MRS Bulletin*, 39(August):668–677, 2014.

[74] A. M. Glushenkov, H. Z. Zhang, J. Zou, G. Q. Lu, and Y. Chen. Efficient production of ZnO nanowires by a ball milling and annealing method. *Nanotechnology*, 18(17), 2007.

[75] A.A. Leonardi, M.J.L. Faro, and A. Irrera. Silicon nanowires synthesis by metal-assisted chemical etching: A review. *Nanomaterials*, 11(2), 2021.

[76] D. Spirkoska, C. Colombo, M. Heiss, G. Abstreiter, and A. Fontcuberta I Morral. The use of molecular beam epitaxy for the synthesis of high purity III-V nanowires. *Journal of Physics Condensed Matter*, 20(45), 2008.

[77] W. Seifert, M. Borgström, K. Deppert, K.A. Dick, J. Johansson, M.W. Larsson, T. Mårtensson, N. Skold, C.P.T. Svensson, B.A. Wacaser, L.R. Wallenberg, and L. Samuelson. Growth of one-dimensional nanostructures in MOVPE. *Journal of Crystal Growth*, 272(1-4 SPEC. ISS.):211–220, 2004.

[78] D.B. Suyatin, W. Hällström, L. Samuelsson, L. Montelius, and C.N. Prinz. Gallium phosphide nanowire arrays and their possible application in cellular force

investigations . *Journal of Vacuum Science Technology B: Microelectronics and Nanometer Structures Processing, Measurement, and Phenomena*, 27:3092–3094, 2009.

[79] J. Valderas-Gutiérrez, R. Davtyan, S. Sivakumar, N. Anttu, Y. Li, P. Flatt, J.Y. Shin, C.N. Prinz, H. Fredrik, T. Fioretos, and M.H. Magnusson. Enhanced Optical Biosensing by Aerotaxy Ga(As)P Nanowire Platforms Suitable for Scalable Production. *ACS Applied Nano Materials*, 5:9063–9071, 2022.

[80] U.W. Pohl. *Introduction*, pages 1–9. Springer Berlin Heidelberg, Berlin, Heidelberg, 2013.

[81] K. Tomioka, K. Ikejiri, T. Tanaka, J. Motohisa, S. Hara, K. Hiruma, and T. Fukui. Selective-area growth of III-V nanowires and their applications. *Journal of Materials Research*, 26(17):2127–2141, 2011.

[82] C. Pendyala, S. Vaddiraju, J.H. Kim, J. Jacinski, Z. Chen, and M.K. Sunkara. Self-nucleation and growth of group III-antimonide nanowires. *Semiconductor Science and Technology*, 25(2), 2010.

[83] M. Heurlin, D. Lindgren, K. Deppert, L. Samuelson, M.H. Magnusson, M. Ek, and L.R. Wallenberg. Continuous gas-phase synthesis of nanowires with tunable properties. *Nature*, 492(7427):90–94, 2012.

[84] S. Sivakumar, A.R. Persson, W. Metaferia, M. Heurlin, R. Wallenberg, L. Samuelson, K. Deppert, J. Johansson, and M.H. Magnusson. Aerotaxy: gas-phase epitaxy of quasi 1D nanostructures. *Nanotechnology*, 32(2), 2021.

[85] M. Yazawa, M. Koguchi, A. Muto, M. Ozawa, and K. Hiruma. Effect of one monolayer of surface gold atoms on the epitaxial growth of InAs nanowhiskers. *Applied Physics Letters*, 61(17):2051–2053, 1992.

[86] K.W. Kolasinski. Catalytic growth of nanowires: Vapor-liquid-solid, vapor-solid-solid, solution-liquid-solid and solid-liquid-solid growth. *Current Opinion in Solid State and Materials Science*, 10(3-4):182–191, 2006.

[87] I. Regolin, V. Khorenko, W. Prost, F.J. Tegude, D. Sudfeld, J. Kästner, and G. Dumpich. Composition control in metal-organic vapor-phase epitaxy grown InGaAs nanowhiskers. *Journal of Applied Physics*, 100(7), 2006.

[88] T. Fukui, M. Yoshimura, E. Nakai, and K. Tomioka. Position-controlled III-V compound semiconductor nanowire solar cells by selective-area metal-organic vapor phase epitaxy. *Ambio*, 41(SUPPL.2):119–124, 2012.

[89] T.F. Kuech. Recent advances in metal-organic vapor phase epitaxy. *Proceedings of the IEEE*, 80(10):1609–1624, 1992.

[90] G.B. Stringfellow. 1 - overview of the omvpe process. In G.B. Stringfellow, editor, *Organometallic Vapor-Phase Epitaxy (Second Edition)*, pages 1–16. Academic Press, San Diego, second edition edition, 1999.

[91] R.S. Wagner and W.C. Ellis. Vapor - liquid - solid mechanism of single crystal growth. *Applied Physics Letters*, 4(June):3–5, 2004.

[92] Kimberly A. Dick, Knut Deppert, Lisa S. Karlsson, L. Reine Wallenberg, Lars Samuelson, and Werner Seifert. A new understanding of au-assisted growth of III-V semiconductor nanowires. *Advanced Functional Materials*, 15(10):1603–1610, 2005.

[93] A. Berg, S. Lehmann, N. Vainorius, A. Gustafsson, M.-E. Pistol, L.R. Wallenberg, L. Samuelson, and M.T. Borgström. Growth and characterization of wurtzite GaP nanowires with control over axial and radial growth by use of HCl in-situ etching. *Journal of Crystal Growth*, 386:47–51, 2013.

[94] A. Berg, K. Mergenthaler, M. Ek, M.-E. Pistol, L.R. Wallenberg, and M.T. Borgström. ¡i¿In situ¡/i¿ etching for control over axial and radial III-V nanowire growth rates using HBr. *Nanotechnology*, 25(50):505601, dec 2014.

[95] S.N. Mohammad. Analysis of the vapor-liquid-solid mechanism for nanowire growth and a model for this mechanism. *Nano Letters*, 8(5):1532–1538, 2008.

[96] H.J. Joyce, Q. Gao, H.H. Tan, C. Jagadish, Y. Kim, M.A. Fickenscher, S. Perera, T.B. Hoang, L.M. Smith, H.E. Jackson, J.M. Yarrison-Rice, X. Zhang, and J. Zou. Unexpected benefits of rapid growth rate for III-V nanowires. *Nano Letters*, 9(2):695–701, 2009.

[97] G. Meng, T. Yanagida, H. Yoshida, K. Nagashima, M. Kanai, F. Zhuge, Y. He, A. Klamchuen, S. Rahong, X. Fang, S. Takeda, and T. Kawai. A flux induced crystal phase transition in the vapor–liquid–solid growth of indium-tin oxide nanowires. *Nanoscale*, 6:7033–7038, 2014.

[98] D.E Perea, N. Li, R.M. Dickerson, A. Misra, and S.T. Picraux. Controlling Heterojunction Abruptness in VLS-Grown Semiconductor. *Nano Letters*, (3):3117–3122, 2011.

[99] K. Hillerich, K.A. Dick, M.E. Messing, K. Deppert, and J. Johansson. Simultaneous Growth Mechanisms for Cu-Seeded InP Nanowires. *Nano Research*, 5(5):297–306, 2012.

[100] S.V. Thombare, A.F. Marshall, and P.C. McIntyre. Size effects in vapor-solid-solid Ge nanowire growth with a Ni-based catalyst. *Journal of Applied Physics*, 054325(December), 2013.

[101] C.B Maliakkal, M. Tornberg, S. Lehmann, K.A. Dick, and D. Jacobsson. Vapor–solid–solid growth dynamics in GaAs nanowires. *Nanoscale Advances*, 3:5928–5940, 2021.

[102] K.A. Dick. A review of nanowire growth promoted by alloys and non-alloying elements with emphasis on Au-assisted III-V nanowires. *Progress in Crystal Growth and Characterization of Materials*, 54(3-4):138–173, 2008.

[103] M.E. Messing, K. Hillerich, J. Johansson, K. Deppert, and K.A. Dick. The use of gold forfabrication of nanowire structres. *Gold Bulletin*, 42(3):172–181, 2009.

[104] R.B. Bedford, C.S.J. Cazin, and D. Holder. The development of palladium catalysts for CC and Cheteroatom bond forming reactions of aryl chloride substrates. *Coordination Chemistry Reviews*, 248(21-24):2283–2321, 2004.

[105] L. Yin and J. Liebscher. Carbon-carbon coupling reactions catalyzed by heterogeneous palladium catalysts. *Chemical Reviews*, 107(1):133–173, 2007.

[106] E. Antolini. Palladium in fuel cell catalysis. *Energy and Environmental Science*, 2(9):915–931, 2009.

[107] R. Chinchilla and C. Nájera. Chemicals from alkynes with palladium catalysts. *Chemical Reviews*, 114(3):1783–1826, 2014.

[108] H. Liu, S. Xue, Y. Tao, W. Long, and S. Zhong. Design and solderability characterization of novel au–30ga solder for high-temperature packaging. *Journal of Materials Science: Materials in Electronics*, 31, 02 2020.

[109] H. Okamoto. Ga-Pd (Gallium-Palladium). *Journal of Phase Equilibria and Diffusion*, 29(5):466–467, 2008.

[110] L.S. Karlsson, M.W. Larsson, J.-O. Malm, and L.R. Wallenberg. Crystal structure of branched epitaxial III-V nanotrees. *NANO: Brief Reports and Reviews*, 1(2):139–151, 2006.

[111] L.D. Pachón and G. Rothenberg. Transition-metal nanoparticles: Synthesis, stability and the leaching issue. *Applied Organometallic Chemistry*, 22(6):288–299, 2008.

[112] R. Narayanan and M.A. El-sayed. Changing Catalytic Activity during Colloidal Platinum Nanocatalysis Due to Shape Changes : Electron-Transfer Reaction. *J. Am. Chem. Soc*, (126):7194–7195, 2004.

[113] M.A. Newton, C. Belver-Coldeira, A. Martínez-Arias, and M. Fernández-García. Dynamic in situ observation of rapid size and shape change of supported Pd nanoparticles during CO/NO cycling. *Nature Materials*, 6(7):528–532, 2007.

[114] Rocío Redón, Nidia G G Peña, and Fermín R Crescencio. Leaching in Metal Nanoparticle Catalysis. *Recent Patents on Nanotechnology*, 8:31–51, 2014.

[115] World Health Organization. Environmental health criteria 226, palladium. *World Health Organization, International Programme on Chemical Safety, Geneva*, 2002.

[116] S. Sisodiya, L.R. Wallenberg, E. Lewin, and O.F. Wendt. Sonogashira coupling reaction over supported gold nanoparticles: Influence of support and catalyst synthesis route. *Applied Catalysis A: General*, 503:69–76, 2015.

[117] P.T. Nilsson, M. Jørgensen, A.B. Yankovich, H. Grönbeck, and E. Olsson. Influence of atomic site-specific strain on catalytic activity of supported nanoparticles. *Nature Communications*, 9(1), 2018.

[118] K. de Haan, Z.S. Ballard, Y. Rivenson, and Y. Wu. Resolution enhancement in scanning electron microscopy using deep learning. *Scientific Reports*, (March):1–7, 2019.

[119] F. Zaera. New Challenges in Heterogeneous Catalysis for the 21st Century. *Catalysis Letters*, 142:501–516, 2012.

[120] S. Nishimura. Handbook of heterogeneous catalytic hydrogenation for organic synthesis john wiley & sons. *Inc.: Hoboken, NJ, USA*, 2001.

[121] W. Bonrath, J. Medlock, J. Schütz, B. Wüstenberg, and J. Netscher. *Hydrogenation in the Vitamins and Fine Chemical Industry - An Overview*, chapter 3, pages 69–90. IntechOpen, 2012.

[122] R. Newhook R. R. Miller and A. Poole. Styrene production, use, and human exposure. *Critical Reviews in Toxicology*, 24(sup1):S1–S10, 1994.

[123] J.M. Thomas. Heterogeneous catalysis: Enigmas, illusions, challenges, realities, and emergent strategies of design. *Journal of Chemical Physics*, 128(18), 2008.

[124] M. Boudart. Heterogeneous catalysis by metals. *Journal of Molecular Catalysis*, 30(1-2):27–38, 1985.

[125] A.L. Walter, F. Schiller, M. Corso, L.R. Merte, F. Bertram, J. Lobo-Checa, M. Shipilin, J. Gustafson, E. Lundgren, A.X. Bríon-Ríos, P. Cabrera-Sanfelix, D. Sánchez-Portal, and J.E. Ortega. X-ray photoemission analysis of clean and carbon monoxide-chemisorbed platinum(111) stepped surfaces using a curved crystal. *Nature Communications*, 6:1–7, 2015.

[126] C. Badan, R.G. Farber, Y. Heyrich, M.T.M. Koper, D.R. Killelea, and L.B.F. Juurlink. Step-Type Selective Oxidation of Platinum Surfaces. *Journal of Physical Chemistry C*, 120(40):22927–22935, 2016.

[127] S. Chen, F. Xiong, and W. Huang. Surface chemistry and catalysis of oxide model catalysts from single crystals to nanocrystals. *Surface Science Reports*, 74(4):100471, 2019.

[128] R. Westerström, M. E. Messing, S. Blomberg, A. Hellman, H. Grönbeck, J. Gustafson, N. M. Martin, O. Balmes, R. Van Rijn, J. N. Andersen, K. Deppert, H. Bluhm, Z. Liu, M. E. Grass, M. Hävecker, and E. Lundgren. Oxidation and reduction of Pd(100) and aerosol-deposited Pd nanoparticles. *Physical Review B - Condensed Matter and Materials Physics*, 83(11):1–10, 2011.

[129] H.-U. Blaser, H. Steiner, and M. Studer. Selective Catalytic Hydrogenation of Functionalized Nitroarenes : An Update. *ChemCatChem*, 1:210–221, 2009.

[130] H. Lindlar. Ein neuer Katalysator für selektive Hydrierungen. *Helvetica Chimica Acta*, 35(2):446–450, feb 1952.

[131] H. Lindlar and R. Dubuis. Process for selective Hydrogenation, 1973.

[132] P. Mcneice, M.-A. Mu, J. Medlock, W. Bonrath, N. Rockstroh, S. Bartling, H. Lund, K. Junge, and M. Beller. Designing a Green Replacement for the Lindlar Catalyst for Alkyne Semi-hydrogenation Using Silica-Supported Nickel Nanoparticles Modified by N-Doped Carbon. *ACS Sustainable Chem. Eng.*, pages 9787–9797, 2022.

[133] J.J. Liu. Advanced Electron Microscopy of Metal-Support Interactions in Supported Metal Catalysts. *ChemCatChem*, 3(6):934–948, 2011.

[134] J. Rebek and F. Gaviña. The Three-Phase Test for Reactive Intermediates. Cyclobutadiene. *Journal of the American Chemical Society*, 96(22):7112–7114, 1974.

[135] R.D. Bach and R.N. Brummel. The Three-Phase Test for Reaction Intermediates. Nucleophilic Catalysis and Elimination Reactions. *Journal of the American Chemical Society*, 97(2):454–455, 1975.

[136] Y. Xin, S. Li, Y. Qian, W. Zhu, H. Yuan, P. Jiang, R. Guo, and L. Wang. High-Entropy Alloys as a Platform for Catalysis : Progress , Challenges , and Opportunities. *ACS Catalysis*, (10):11280–11306, 2020.

Printed by Media-Tryck, Lund 2023 NORDIC SWAN ECOLABEL 3041 0903

The energy landscape of a catalytic process can be related to a mountain range, with many possible pathways downwards.

Lund University
Faculty of Engineering
Department of Physics

ISBN 978-91-8039-890-9